AN EXACT MODAL ANALYSIS APPROACH TO VIBRATION ANALYSIS OF STRUCTURES WITH MASS-SPRING SUBSYSTEMS AND ROTATIONAL JOINTS

Giuseppe Failla
Department of Civil, Energy, Environmental and Materials Engineering (DICEAM)
University of Reggio Calabria, Via Graziella, 89124 Reggio Calabria, Italy
Email: giuseppe.failla@unirc.it

ABSTRACT

A novel exact modal analysis approach is presented for vibration analysis of plane continuous structures, which are coupled with discrete mass-spring subsystems and include elastic rotational joints modelling local flexibility. Using the theory of generalised functions to handle the discontinuities of the response variables, every continuous member with any number of mass-spring subsystems and joints is treated as a two-node element, for which a 6×6 exact dynamic stiffness matrix is obtained in closed form. As a result, the global dynamic stiffness matrix is built by a standard finite-element assembling procedure, with size depending only on the number of nonzero nodal degrees of freedom of member-to-member nodes. Upon deriving pertinent orthogonality conditions for the modes, the system response under arbitrary loads is obtained by modal impulse and modal frequency response functions, under the assumption of proportional damping. The solutions are exact and can be used as benchmark for classical finite-element solutions. The approach is formulated for various mass-spring subsystems, acting in transverse and axial directions relative to every member.

KEYWORDS: Modal Analysis, Dynamic Stiffness Matrix, Euler-Bernoulli Beam, Mass-Spring Subsystem, Elastic Rotational Joint.

1. INTRODUCTION

The dynamics of continuous structures coupled with discrete mass-spring subsystems is of strong interest in structural and mechanical applications. Mass-spring subsystems are used to model engines, machineries and, more generally, secondary structures whose motion is coupled with that of the primary continuous one (e.g., see ref. [1] and list of references therein). Combinations of beams with multiple mass-spring subsystems are involved in passive vibration control [2-6] and

also human-structure interaction [7,8]. In view of the large number of applications, a considerable number of studies has been devoted to this subject, considering free as well as forced vibrations [1-30].

The bending response of single beams coupled with various mass-spring subsystems has been investigated by several authors [5-26]. Studies have considered one-mass-one-spring subsystems [9-16], multi-mass-multi-spring subsystems [17,18], two-mass-one-spring subsystems [13] as well as lumped masses attached to the beam [19-21]. Some authors have examined beams with one-mass-one-spring subsystems, elastic external supports and internal joints [22,23], as well as stepwise changes in the cross-section properties [24]. Recent studies have dealt with stepped beams carrying three-mass-three-spring subsystems [25] where one spring is grounded, or one-mass-one-spring subsystems [26], considering the effect of axial load. The authors have generally focused on free vibrations as primary goal for design purposes, using various methods for computing the undamped modes: assumed-mode method [5-7,9,10,13,15,17], analytical approaches with Green's functions of the bare beam [14,16,18,19], Laplace Transform of motion equation [20,22], an equivalent-center method [21], a numerical assembly technique [11,23], the transfer matrix approach [8,24,26]. Scope of most studies in ref. [5-26] was an efficient formulation of the eigenvalue problem, in general reducing the size of the matrix whose determinant provides the characteristic equation or, in some cases, deriving the latter in closed analytical form. Also forced vibrations have been addressed: the vibration suppression effect of several one-mass-one-spring subsystems attached to a beam subjected to transverse harmonic excitation was investigated by Cha [5,6], using the assumed-mode method. As for the axial response, free vibrations of single rods coupled with one-mass-one-spring subsystems and carrying lumped masses have been studied [27,28], deriving exact and approximate characteristic equations [27] as well as methods for sensitivity analyses of the natural frequencies [28].

A few studies have been devoted to free and forced vibrations of plane/space continuous structures coupled with mass-spring subsystems. Space structures with one-mass-one-spring subsystems have been studied by Guo and Chen [29] using the reverberation matrix approach in conjunction with generalised matrix inversion to compute undamped modes and frequency response matrix. Forced vibrations were investigated by impulse response functions obtained as inverse Fourier Transform of the frequency response matrix [29]. The same authors have applied the reverberation matrix approach for modal analysis of space structures with lumped masses and elastic springs and, in this case, pertinent orthogonality conditions of the undamped modes were derived to investigate time and frequency response to arbitrary loads [30]. The reverberation matrix approach requires considering a node at every location of a mass-spring subsystem, lumped mass,

elastic spring or point load, while continuous members are interconnected at the nodes. In ref. [1], Banerjee proposed an exact dynamic stiffness matrix approach [31] for the free vibration problem of plane structures with one-mass-one-spring subsystems. Dias and Alves [32,33] developed an original exact method for free vibration analysis of plane structures involving continuous members that may incorporate rigid offsets and/or end releases at the member-to-member nodes, where, in addition, elastic springs and lumped masses may be attached. The approach calculates natural frequencies and undamped modes from an eigenvalue problem including the degrees of freedom of the member-to-member nodes as well as the integration constants associated with the exact free vibration response within every member. This is a straightforward way to calculate global and local modes (i.e. modes involving member displacements but zero nodal displacements) using efficient numerical algorithms, as for instance the secant method [32,33]. The method by Dias and Alves [32,33] has relevant advantages with respect to a classical dynamic stiffness approach with equilibrium equations written at the member-to-member nodes because, in the latter, local modes are associated with the poles of the global dynamic stiffness matrix and cannot be calculated directly from the equilibrium equations. On the other hand, the authors pointed out that even adapted versions of the dynamic stiffness matrix approach, where poles are eliminated, would require further developments to include rigid offsets and/or end releases and determine the related local mode shapes [32,33]. The method applies for Euler-Bernoulli [32] as well as shear-deformable Timoshenko members [33]. Timoshenko plane structures in ref. [33], with rigid offsets and end releases along the members, were further addressed in ref. [34] with focus on forced vibrations under harmonic loads; in this case the exact frequency response was calculated by pertinent global dynamic stiffness matrix and load vector built by a Laplace transform approach.

Other studies on plane structures have concerned free vibrations when elastic rotational joints [35,36] or deflection/rotation/axial-displacement joints [37] are arbitrarily located along the members, using the theory of generalised functions. The effect of axial load on the free vibrations of plane structures, in presence of elastic rotational joints modelling cracks, was investigated by Caddemi et al. [38]. In this case, the difficulty was to solve the Euler-Bernoulli beam bending equation with additional terms accounting for axial load effect and rotation discontinuities associated with cracks. The authors obtained straightforward exact solutions using the theory of generalised functions [38]. On this basis they derived explicit, closed analytical expressions for the 4×4 dynamic stiffness matrix of a two-node beam-column member which, remarkably, holds the same size for any number and positions of cracks [38].

Obviously, a most general method for handling free and forced vibrations of plane/space structures coupled with mass-spring subsystems, possibly including internal joints, is a standard

two-node finite-element (FE) method. However, there are some disadvantages in a FE approach: the solution is approximate and accuracy needs to be checked with mesh refinement; also, a node shall be considered at the application point of every mass-spring subsystem/joint as well as point load, and re-meshing is required if positions of mass-spring subsystems/joints/loads vary, as is typically the case in sensitivity and optimization analyses.

This paper proposes a novel exact modal analysis approach to vibration analysis of plane continuous structures, which are coupled with discrete mass-spring subsystems and include elastic rotational joints modelling local flexibility [35,36,38,39]. The approach is presented for various types of mass-spring subsystems considered in the literature [1-30], acting in transverse and axial directions relative to every continuous member. For the latter, the Euler-Bernoulli beam theory is adopted.

The first step of the paper is to show that, using pertinent generalised functions [40-42] within a well-established dynamic stiffness approach to the modelling of plane structures with cracks, rigid offsets and various types of attachments along the members [32-36,38,43-45], every member with any number of mass-spring subsystems and joints can be treated as a two-node element, for which a 6×6 exact dynamic stiffness matrix is derived in closed form. In this manner, a standard FE assembly procedure provides a global dynamic stiffness matrix with size depending only on the number of nonzero nodal degrees of freedom of member-to-member nodes. From the global dynamic stiffness matrix, the exact natural frequencies of the undamped modes can be computed, e.g. using the well-known Wittrick-Williams (W-W) algorithm [46,47]. Then, on deriving pertinent orthogonality conditions for the modes, closed-form expressions are obtained for modal impulse and modal frequency response functions, to be used for forced vibration analysis under arbitrary loads, under the assumption of proportional damping. The solutions are exact and serve as benchmark for classical FE solutions. The analytical form is simple and can readily be implemented regardless of number of mass-spring subsystems, joints and loads along every member.

The paper is organized as follows. The structures under study are described in Section 2. The dynamic stiffness matrix approach to free vibrations is described in Section 3. Orthogonality conditions for the modes are derived in Section 4, while forced vibration analysis is discussed in Section 5. A numerical application is presented in Section 6. Finally, one Appendix is included.

2. PROBLEM STATEMENT

Figure 1 shows a plane structure involving uniform Euler-Bernoulli continuous members coupled with various mass-spring subsystems, acting in transverse and axial directions relative to every member. In addition, elastic rotational joints are considered, modelling local flexibility [35,36,38].

For generality, it is assumed that an arbitrary number of mass-spring subsystems and joints may exist along every member. The system is acted upon by nodal and distributed dynamic loads.

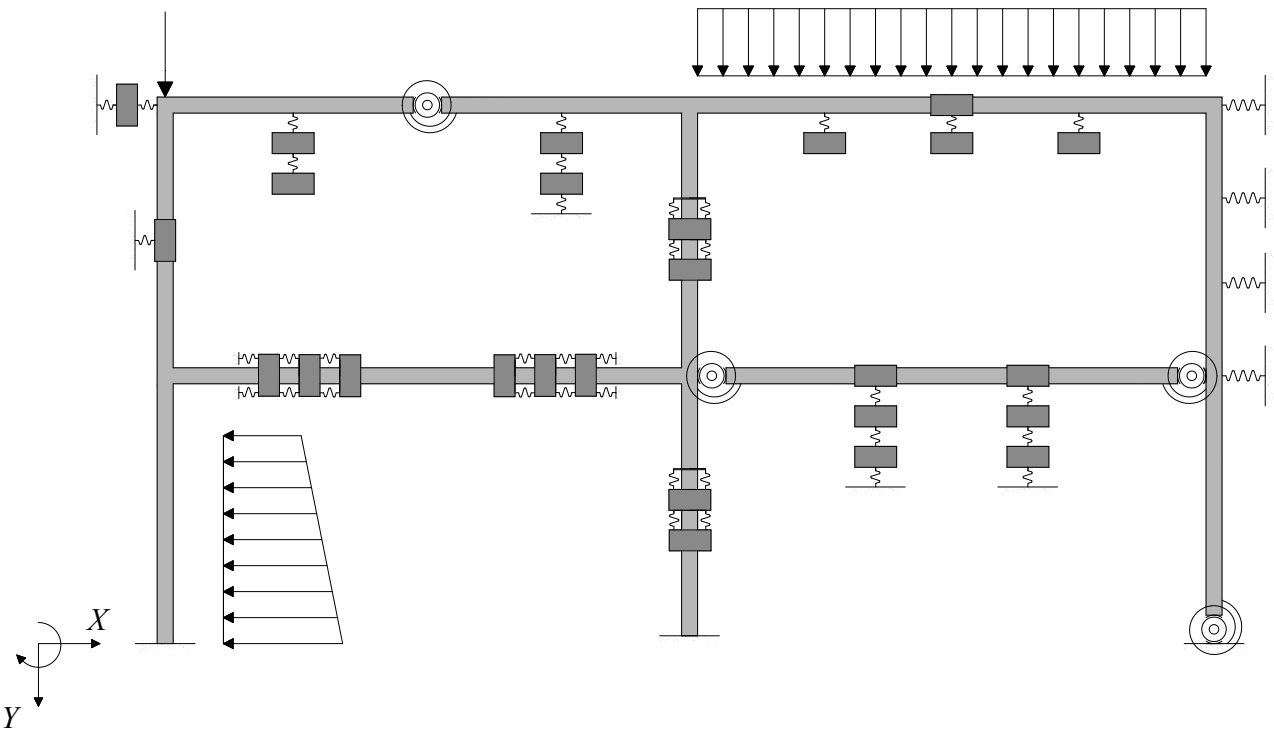

Figure 1. Plane structure composed of uniform Euler-Bernoulli continuous members coupled with discrete mass-spring subsystems and including elastic rotational joints.

The equations of motion will be written assuming that the mass-spring subsystems along the ith member are three-mass-three-spring subsystems connected to the member as well as to ground, as shown in Figure 2. It will be shown that solutions obtained for the three-mass-three-spring subsystem include those for the other mass-spring subsystems in Figure 1, with appropriate choice of parameters in Figure 2. In Figure 2, $L^{(i)}$ = length, $EI^{(i)}$ = flexural stiffness, $EA^{(i)}$ = axial stiffness, $\rho^{(i)}$ = mass per unit length of the ith member.

Another simplifying assumption in the formulation is that a mass-spring subsystem and a joint occur simultaneously at every location $x_j^{(i)}$. However, changes to consider either a mass-spring subsystem or a joint only occur at a given $x_j^{(i)}$ will be straightforward, as shown later in the paper.

As for notation, response variables in the local coordinate system of every member will be denoted by (˜), to be distinguished by those in the global coordinate system (global and local coordinate systems are shown in Figure 1 and Figure 2 respectively; positive sign conventions for

response variables are given in Figure 2). The local abscissa will be denoted as x, without superscript (i) for brevity.

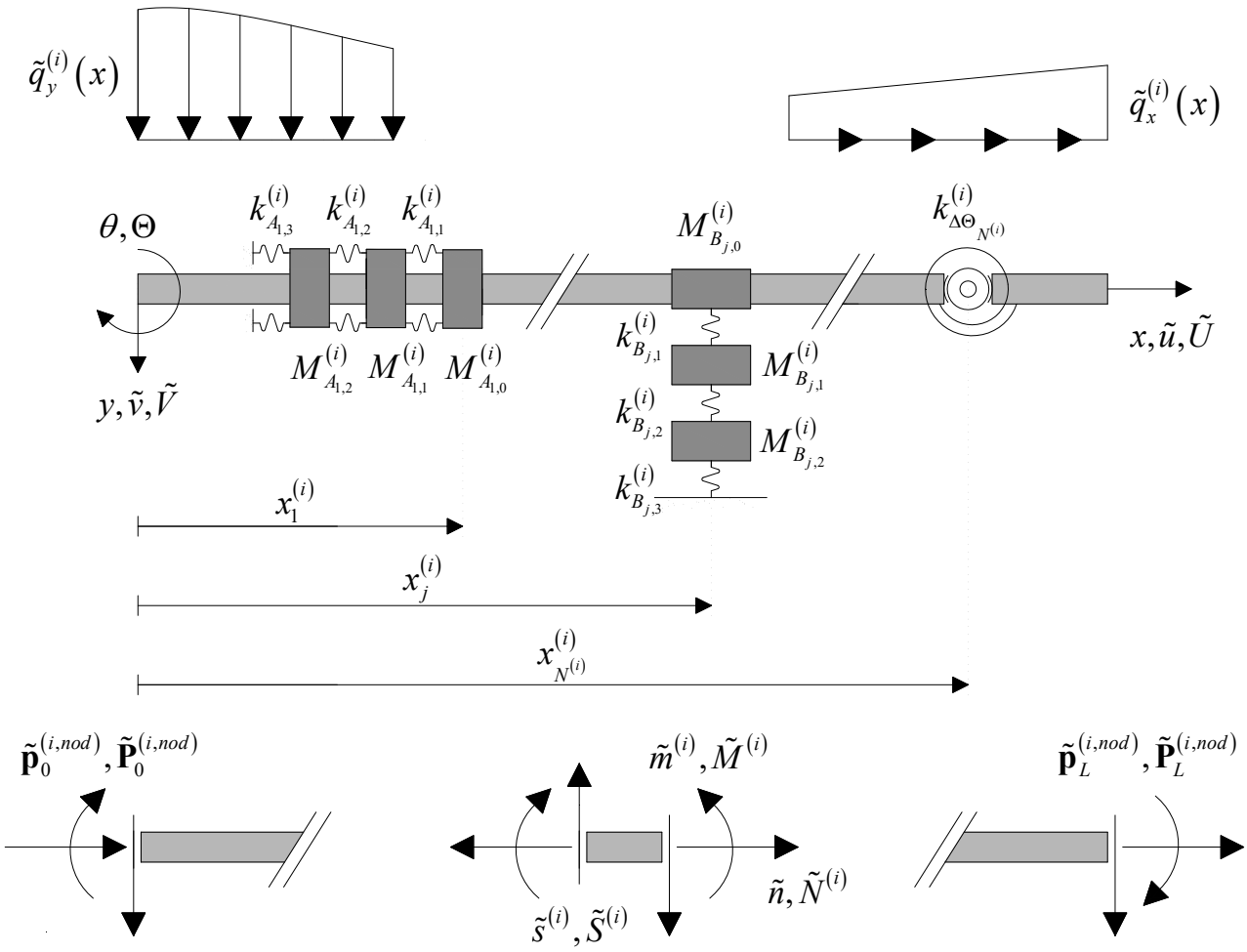

Figure 2. Euler-Bernoulli continuous member with arbitrary number of discrete mass-spring subsystems and elastic rotational joints. Parameters and positive sign conventions are shown.

3. FREE VIBRATIONS

As a first step of the study, consider the free vibrations of the plane structure in Figure 1.

For every mode, the deflection of the ith member in the local coordinate system can be represented as $\tilde{v}^{(i)}(x,t) = \tilde{V}^{(i)}(x)\mathrm{e}^{\mathrm{i}\omega t}$ (i = imaginary unit, ω = modal frequency), where $\tilde{V}^{(i)}(x)$ is the deflection eigenfunction governed by the following 4th order differential equation:

$$EI^{(i)} \frac{\overline{\mathrm{d}}^4 \tilde{V}^{(i)}(x)}{\mathrm{d}x^4} - \tilde{B}^{(i)}(x) - \rho^{(i)}\omega^2 \tilde{V}^{(i)}(x) = 0 \tag{1}$$

$$\tilde{B}^{(i)}(x)=\sum_{j=1}^{N^{(i)}}\tilde{R}_{B_j}^{(i)}\left(\tilde{V}^{(i)}\right)\delta\left(x-x_j^{(i)}\right)+\sum_{j=1}^{N^{(i)}}EI^{(i)}\Delta\tilde{\Theta}_j^{(i)}\left(\tilde{M}^{(i)}\right)\delta^{(2)}\left(x-x_j^{(i)}\right) \tag{2}$$

In Eqs.(1)-(2), bar means generalised derivative, symbols $\delta\left(x-x_j^{(i)}\right)$ and $\delta^{(2)}\left(x-x_j^{(i)}\right)$ denote a Dirac's delta and its 2nd formal derivative at $x=x_j^{(i)}$. Further, $\Delta\tilde{\Theta}_j^{(i)}$ is the relative rotation between adjacent sections of the elastic rotational joint at $x=x_j^{(i)}$, while $\tilde{R}_{B_j}^{(i)}\left(\tilde{V}^{(i)}\right)$ is the transverse force exerted by the mass-spring subsystem applied at $x=x_j^{(i)}$,

$$\Delta\tilde{\Theta}_j^{(i)}\left(\tilde{M}^{(i)}\right)=-\left(k_{\Delta\Theta_j}^{(i)}\right)^{-1}\tilde{M}^{(i)}\left(x_j^{(i)}\right) \tag{3}$$

$$\tilde{R}_{B_j}^{(i)}\left(\tilde{V}^{(i)}\right)=-\kappa_{B_j}^{(i)}(\omega)\tilde{V}^{(i)}\left(x_j^{(i)}\right) \tag{4}$$

being $\kappa_{B_j}^{(i)}(\omega)$ a frequency-dependent stiffness of the mass-spring subsystem given by

$$\kappa_{B_j}^{(i)}(\omega)=\frac{k_{B_{j,1}}^{(i)}\left(k_{B_{j,3}}^{(i)}M_{B_{j,1}}^{(i)}\omega^2+k_{B_{j,2}}^{(i)}\left(\left(M_{B_{j,1}}^{(i)}+M_{B_{j,2}}^{(i)}\right)\omega^2-k_{B_{j,3}}^{(i)}\right)-M_{B_{j,1}}^{(i)}M_{B_{j,2}}^{(i)}\omega^4\right)}{\left(k_{B_{j,2}}^{(i)}\right)^2-\left(M_{B_{j,1}}^{(i)}\omega^2-k_{B_{j,1}}^{(i)}-k_{B_{j,2}}^{(i)}\right)\left(M_{B_{j,2}}^{(i)}\omega^2-k_{B_{j,2}}^{(i)}-k_{B_{j,3}}^{(i)}\right)}-M_{B_{j,0}}^{(i)}\omega^2 \tag{5}$$

Eq.(5) holds because the transverse force $\tilde{R}_{B_j}^{(i)}\left(\tilde{V}^{(i)}\right)$ in Eq.(4) involves the inertia force acting on mass $M_{B_{j,0}}^{(i)}$ as well as the elastic force of the spring with stiffness $k_{B_{j,1}}^{(i)}$, and both forces can be expressed as functions of the deflection $\tilde{V}^{(i)}\left(x_j^{(i)}\right)$ of the application point only; for the elastic force, this is feasible using the free-vibration equilibrium equations of masses $M_{B_{j,1}}^{(i)}, M_{B_{j,2}}^{(i)}$ to express the displacement of mass $M_{B_{j,1}}^{(i)}$ in terms of $\tilde{V}^{(i)}\left(x_j^{(i)}\right)$, for every mode [17,18]. It is noteworthy that different types of mass-spring subsystems examined in the literature and shown in Figure 1 can be handled by Eqs.(4)-(5) with simple changes. For instance, the frequency-dependent stiffness of a mass *M* attached to the beam by a spring with stiffness *k* [9-14,22-23] can be obtained from Eq.(5) setting $M_{B_{j,0}}^{(i)}=M_{B_{j,1}}^{(i)}=k_{B_{j,3}}^{(i)}=0$, replacing $k_{B_{j,1}}^{(i)}k_{B_{j,2}}^{(i)}\Big/\left(k_{B_{j,1}}^{(i)}+k_{B_{j,2}}^{(i)}\right)$ by *k* and $M_{B_{j,2}}^{(i)}$ by *M*; a grounded

spring with stiffness k [1,22] can be treated using Eq.(5) where $M_{B_{j,0}}^{(i)} = M_{B_{j,1}}^{(i)} = M_{B_{j,2}}^{(i)} = 0$ and $k_{B_{j,1}}^{(i)} k_{B_{j,2}}^{(i)} k_{B_{j,3}}^{(i)} \Big/ \left(k_{B_{j,1}}^{(i)} k_{B_{j,2}}^{(i)} + k_{B_{j,1}}^{(i)} k_{B_{j,3}}^{(i)} + k_{B_{j,2}}^{(i)} k_{B_{j,3}}^{(i)} \right)$ is replaced by k. Similar changes hold for the other mass-spring subsystems in Figure 1 and treated, among others, in ref. [13,15-18,24].

As for axial vibrations, for every mode the axial displacement of the ith member in the local coordinate system can be represented as $\tilde{u}^{(i)}(x,t) = \tilde{U}^{(i)}(x)\mathrm{e}^{\mathrm{i}\omega t}$, with $\tilde{U}^{(i)}(x)$ axial-displacement eigenfunction governed by the 2nd order differential equation:

$$EA^{(i)} \frac{\overline{\mathrm{d}}^2 \tilde{U}^{(i)}(x)}{\mathrm{d}x^2} + \tilde{A}^{(i)}(x) + \rho^{(i)} \omega^2 \tilde{U}^{(i)}(x) = 0 \tag{6}$$

$$\tilde{A}^{(i)}(x) = \sum_{j=1}^{N^{(i)}} \tilde{R}_{A_j}^{(i)}\left(\tilde{U}^{(i)}\right) \delta\left(x - x_j^{(i)}\right) \tag{7}$$

In Eq.(7), $\tilde{R}_{A_j}^{(i)}\left(\tilde{U}^{(i)}\right)$ mirrors $\tilde{R}_{B_j}^{(i)}\left(\tilde{V}^{(i)}\right)$ in Eq.(4) for the bending problem, i.e.

$$\tilde{R}_{A_j}^{(i)}\left(\tilde{U}^{(i)}\right) = -\kappa_{A_j}^{(i)}(\omega) \tilde{U}^{(i)}\left(x_j^{(i)}\right) \tag{8}$$

where $\kappa_{A_j}^{(i)}(\omega)$ takes the same form as $\kappa_{B_j}^{(i)}(\omega)$ in Eq.(5), with $k_{B_{j,k}}^{(i)}, M_{B_{j,k}}^{(i)}$ replaced by the corresponding parameters pertinent to the axial problem, i.e. $k_{A_{j,k}}^{(i)}$, $M_{A_{j,k}}^{(i)}$. Obviously, Eq.(8) may handle also the various mass-spring subsystems acting in axial direction relative to the members in Figure 1 (see previous comments on Eqs.(4)-(5) for the bending problem).

Next, be $\tilde{\mathbf{Y}}_B^{(i)}(x) = \left\{ \tilde{V}^{(i)}(x) \quad \tilde{\Theta}^{(i)}(x) \quad \tilde{M}^{(i)}(x) \quad \tilde{S}^{(i)}(x) \right\}^T$ and $\tilde{\mathbf{Y}}_A^{(i)}(x) = \left\{ \tilde{U}^{(i)}(x) \quad \tilde{N}^{(i)}(x) \right\}^T$ the vectors collecting the response variables of bending and axial problem, respectively. Following the approach proposed by the author in ref. [45], it can be written that

$$\tilde{\mathbf{Y}}_B^{(i)}(x) = \tilde{\mathbf{W}}_B^{(i)}(x) \mathbf{c}_B^{(i)} \tag{9}$$

$$\tilde{\mathbf{Y}}_A^{(i)}(x) = \tilde{\mathbf{W}}_A^{(i)}(x) \mathbf{c}_A^{(i)} \tag{10}$$

where $\mathbf{c}_B^{(i)} = \left\{ c_{B,1}^{(i)} \quad c_{B,2}^{(i)} \quad c_{B,3}^{(i)} \quad c_{B,4}^{(i)} \right\}^T$ and $\mathbf{c}_A^{(i)} = \left\{ c_{A,1}^{(i)} \quad c_{A,2}^{(i)} \right\}^T$ are vector of integration constants, $\tilde{\mathbf{W}}_B^{(i)}(x)$ and $\tilde{\mathbf{W}}_A^{(i)}(x)$ are 4×4 and 2×2 matrices depending on the solutions to Eq.(1) and Eq.(6). Details on Eqs.(9)-(10) may be found in ref. [45] and are summarized in Appendix A.

Starting from Eqs.(9)-(10) and following a well-established dynamic stiffness approach to the modelling of plane structures with cracks, rigid offsets and attachments along the members [32-36,42-45], the ith member can be considered as a two-node element with nodes at $x = 0$ and $x = L^{(i)}$, for which the following nodal vectors can be defined (see Figure 2):

$$\begin{aligned} \tilde{\mathbf{P}}^{(i,nod)} &= \left\{ \tilde{\mathbf{P}}_0^{(i,nod)} \quad \tilde{\mathbf{P}}_L^{(i,nod)} \right\}^T \\ &= \left\{ -\tilde{N}^{(i)}(0) \quad -\tilde{S}^{(i)}(0) \quad \tilde{M}^{(i)}(0) \quad \tilde{N}^{(i)}\left(L^{(i)}\right) \quad \tilde{S}^{(i)}\left(L^{(i)}\right) \quad -\tilde{M}^{(i)}\left(L^{(i)}\right) \right\}^T \end{aligned} \tag{11}$$

$$\begin{aligned} \tilde{\mathbf{U}}^{(i,nod)} &= \left\{ \tilde{\mathbf{U}}_0^{(i,nod)} \quad \tilde{\mathbf{U}}_L^{(i,nod)} \right\} \\ &= \left\{ \tilde{U}^{(i)}(0) \quad \tilde{V}^{(i)}(0) \quad \tilde{\Theta}^{(i)}(0) \quad \tilde{U}^{(i)}\left(L^{(i)}\right) \quad \tilde{V}^{(i)}\left(L^{(i)}\right) \quad \tilde{\Theta}^{(i)}\left(L^{(i)}\right) \right\}^T \end{aligned} \tag{12}$$

being

$$\tilde{\mathbf{U}}^{(i,nod)} = \tilde{\mathbf{\Gamma}}^{(i)} \mathbf{c}^{(i)} \qquad \tilde{\mathbf{P}}^{(i,nod)} = \tilde{\mathbf{\Xi}}^{(i)} \mathbf{c}^{(i)} \tag{13a,b}$$

for $\mathbf{c}^{(i)} = \left\{ \mathbf{c}_A^{(i)} \quad \mathbf{c}_B^{(i)} \right\}^T$, while $\tilde{\mathbf{\Gamma}}^{(i)}$ and $\tilde{\mathbf{\Xi}}^{(i)}$ are 6×6 matrices involving $\tilde{\mathbf{W}}_B^{(i)}(x)$ and $\tilde{\mathbf{W}}_A^{(i)}(x)$ as computed at $x = 0$ and $x = L^{(i)}$, see again Appendix A.

From Eqs.(13) one obtains

$$\tilde{\mathbf{P}}^{(i,nod)} = \tilde{\mathbf{\Xi}}^{(i)} \left(\tilde{\mathbf{\Gamma}}^{(i)} \right)^{-1} \tilde{\mathbf{U}}^{(i,nod)} = \tilde{\mathbf{D}}^{(i)} \tilde{\mathbf{U}}^{(i,nod)} \tag{14}$$

where $\tilde{\mathbf{D}}^{(i)} = \tilde{\mathbf{D}}^{(i)}(\omega)$ is the frequency-dependent dynamic stiffness matrix of the ith member. Closed-form expressions for every term of $\tilde{\mathbf{D}}^{(i)}$ can be found, as shown in ref. [45] for a similar 6×6 matrix. Notice that, based on Eq.(14), every member of the plane structure in Figure 1 can be considered as a two-node element whose dynamic stiffness matrix holds the size 6×6, regardless of the number of mass-spring subsystems and joints.

Once the 6×6 dynamic stiffness matrix $\tilde{\mathbf{D}}^{(i)}$ is computed for every member, the global dynamic stiffness matrix may be built by a standard FE assembling procedure. Enforcing equilibrium and applying the kinematic boundary conditions yield

$$\mathbf{D}\mathbf{U} = \mathbf{0} \tag{15}$$

where $\mathbf{D} = \mathbf{D}(\omega)$ is the global dynamic stiffness matrix and $\mathbf{U}$ is the vector collecting all nodal displacements in the global coordinate system. That is,

$$\mathbf{D} = \sum_{i=1}^{Ne} \left(\mathbf{L}^{(i)}\right)^T \mathbf{D}^{(i)} \mathbf{L}^{(i)} \tag{16}$$

where *Ne*=number of members, while $\mathbf{D}^{(i)}$ and $\mathbf{L}^{(i)}$ denote respectively the dynamic stiffness matrix of the ith member in the global coordinate system and the connectivity matrix of the ith member, i.e.

$$\mathbf{D}^{(i)} = \left(\mathbf{T}^{(i)}\right)^T \tilde{\mathbf{D}}^{(i)} \mathbf{T}^{(i)} \qquad \text{for} \quad \mathbf{T}^{(i)} = \begin{bmatrix} \cos\varphi^{(i)} & \sin\varphi^{(i)} \\ -\sin\varphi^{(i)} & \cos\varphi^{(i)} \end{bmatrix} \tag{17a,b}$$

and

$$\tilde{\mathbf{U}}^{(i,nod)} = \mathbf{T}^{(i)} \mathbf{U}^{(i,nod)} \qquad \text{for} \qquad \mathbf{U}^{(i,nod)} = \mathbf{L}^{(i)} \mathbf{U} \tag{18a,b}$$

In Eqs.(17)-(18), $\mathbf{T}^{(i)}$ is the transformation matrix for the vector of nodal displacements from global to local coordinate system, being $\varphi^{(i)}$ the angle between local and global coordinate system ($\varphi^{(i)}$ positive clockwise).

The equations derived above slightly modify if external mass-spring subsystems are applied at member-to-member nodes of the plane structure. Assuming that the mass-spring subsystem at node N_k acts along an arbitrary direction $\mathbf{t}^{(N_k)} = \left\{ t_X^{(N_k)} \quad t_Y^{(N_k)} \right\}^T$, $\left\| \mathbf{t}^{(N_k)} \right\| = 1$ in the global coordinate system, the global dynamic stiffness matrix $\mathbf{D}(\omega)$ reads

$$\mathbf{D} = \sum_{i=1}^{Ne} \left(\mathbf{L}^{(i)}\right)^T \mathbf{D}^{(i)} \mathbf{L}^{(i)} + \sum_{N_k} \left(\mathbf{L}^{(N_k)}\right)^T \mathbf{K}^{(N_k)} \mathbf{L}^{(N_k)} \tag{19}$$

where $N_k = N_1, N_2 \ldots$ is an index for the member-to-member nodes with external mass-spring subsystems, $\mathbf{L}^{(N_k)}$ is the connectivity matrix for displacements/rotations of node N_k and $\mathbf{K}^{(N_k)}$ is the dynamic stiffness matrix of the mass-spring subsystem, i.e.

$$\mathbf{K}^{(N_k)}(\omega) = \kappa^{(N_k)}(\omega) \begin{bmatrix} t_X^{(N_k)} t_X^{(N_k)} & t_X^{(N_k)} t_Y^{(N_k)} \\ t_X^{(N_k)} t_Y^{(N_k)} & t_Y^{(N_k)} t_Y^{(N_k)} \end{bmatrix} \tag{20}$$

with $\kappa^{(N_k)}(\omega)$ given, in general, as Eq.(5).

It is remarkable that the size of the global dynamic stiffness matrix given by Eq.(16) or Eq.(19) depends only on the number of nonzero nodal degrees of freedom of member-to-member nodes, regardless of the number of mass-spring subsystems and joints along every member.

All natural frequencies of the plane structure can be computed as roots of the global dynamic stiffness matrix given by Eq.(16) or Eq.(19), e.g. using the well-known W-W algorithm [46,47]. The implementation requires the number J_i of "clamped-clamped" natural frequencies, which fall below any arbitrary trial frequency, of the two-node i^{th} member with mass-spring subsystems and joints. Adopting the approach proposed in a recent paper on frames composed of multi-cracked members [35], J_i can be computed applying the W-W algorithm to every i^{th} member with clamped ends and using, for this specific purpose, its dynamic stiffness matrix built by assembling the dynamic stiffness matrices of member segments connected at the internal points where mass-spring subsystems and/or joints occur; in this context, the dynamic stiffness matrices of the mass-spring subsystems will be assembled with those of the member segments (see example in ref. [1] for a one-mass-one-spring subsystem) and rotational springs will be considered where joints are applied.

For every computed natural frequency ω, the nodal displacement vector $\mathbf{U}$ will be built as non-trivial solution of Eq.(15). Corresponding eigenfunctions $\tilde{\mathbf{Y}}_B^{(i)}(x)$ and $\tilde{\mathbf{Y}}_A^{(i)}(x)$ for all response variables in the ith member will be built from Eqs.(9)-(10), where $\mathbf{c}_B^{(i)}$ and $\mathbf{c}_A^{(i)}$ are obtained by Eqs.(13a) as $\mathbf{c}^{(i)} = \left(\tilde{\mathbf{\Gamma}}^{(i)}\right)^{-1} \tilde{\mathbf{U}}^{(i,nod)}$, with $\tilde{\mathbf{U}}^{(i,nod)} = \mathbf{T}^{(i)}\mathbf{L}^{(i)}\mathbf{U}$, see Eqs.(18). The displacements of the masses in the mass-spring subsystems can readily be computed from deflection/axial-displacement of the application point, using the free-vibration equilibrium equations of the masses (e.g. see ref. [17,18] for pertinent equations).

4. ORTHOGONALITY CONDITIONS

The second step of the study is to show that relevant orthogonality conditions hold for the vibration modes, as explained in this Section.

For the nth mode, be $\tilde{V}_n^{(i)}(x)$, $\tilde{U}_n^{(i)}(x)$ the deflection and axial-displacement eigenfunction of the ith member in the local coordinate system, for which the following equations hold:

$$EI^{(i)}\frac{\overline{\mathrm{d}}^4\tilde{V}_n^{(i)}(x)}{\mathrm{d}x^4}-\tilde{B}_n^{(i)}(x)-\rho^{(i)}\omega_n^2\tilde{V}_n^{(i)}(x)=0 \tag{21}$$

$$EA^{(i)}\frac{\overline{\mathrm{d}}^2\tilde{U}_n^{(i)}(x)}{\mathrm{d}x^2}+\tilde{A}_n^{(i)}(x)+\rho^{(i)}\omega_n^2\tilde{U}_n^{(i)}(x)=0 \tag{22}$$

On multiplying Eq.(21) by deflection $\tilde{V}_m^{(i)}(x)$ and Eq.(22) by axial displacement $\tilde{U}_m^{(i)}(x)$ of the mth mode, integrating over the length $L^{(i)}$ yields

$$EI^{(i)}\int_0^{L^{(i)}}\frac{\overline{\mathrm{d}}^4\tilde{V}_n^{(i)}(x)}{\mathrm{d}x^4}\tilde{V}_m^{(i)}(x)\mathrm{d}x-\int_0^{L^{(i)}}\tilde{B}_n^{(i)}(x)\tilde{V}_m^{(i)}(x)\mathrm{d}x-\rho^{(i)}\omega_n^2\int_0^{L^{(i)}}\tilde{V}_n^{(i)}(x)\tilde{V}_m^{(i)}(x)\mathrm{d}x=0 \tag{23}$$

$$EA^{(i)}\int_0^{L}\frac{\overline{\mathrm{d}}^2\tilde{U}_n^{(i)}(x)}{\mathrm{d}x^2}\tilde{U}_m^{(i)}(x)\mathrm{d}x+\int_0^{L}\tilde{A}_n^{(i)}(x)\tilde{U}_m^{(i)}(x)\mathrm{d}x+\rho^{(i)}\omega_n^2\int_0^{L}\tilde{U}_n^{(i)}(x)\tilde{U}_m^{(i)}(x)\mathrm{d}x=0 \tag{24}$$

On integrating by parts the first integral on the l.h.s., Eq.(23) and Eq.(24) can be recast in the following forms

$$\begin{aligned}&\tilde{S}_n^{(i)}\left(L^{(i)}\right)\tilde{V}_m^{(i)}\left(L^{(i)}\right)-\tilde{S}_n^{(i)}(0)\tilde{V}_m^{(i)}(0)-\tilde{M}_n^{(i)}\left(L^{(i)}\right)\tilde{\Theta}_m^{(i)}\left(L^{(i)}\right)+\tilde{M}_n^{(i)}(0)\tilde{\Theta}_m^{(i)}(0)=\\&+EI^{(i)}\int_0^{L^{(i)}}\frac{\overline{\mathrm{d}}^2\tilde{V}_n^{(i)}(x)}{\mathrm{d}x^2}\frac{\overline{\mathrm{d}}^2\tilde{V}_m^{(i)}(x)}{\mathrm{d}x^2}\mathrm{d}x-\int_0^{L^{(i)}}B_n^{(i)}(x)\tilde{V}_m^{(i)}(x)\mathrm{d}x-\rho^{(i)}\omega_n^2\int_0^{L^{(i)}}\tilde{V}_n^{(i)}(x)\tilde{V}_m^{(i)}(x)\mathrm{d}x\end{aligned} \tag{25}$$

$$\begin{aligned}&\tilde{N}_n^{(i)}\left(L^{(i)}\right)\tilde{U}_m^{(i)}\left(L^{(i)}\right)-\tilde{N}_n^{(i)}(0)\tilde{U}_m^{(i)}(0)=\\&EA^{(i)}\int_0^{L^{(i)}}\frac{\overline{\mathrm{d}}\tilde{U}_n^{(i)}(x)}{\mathrm{d}x}\frac{\overline{\mathrm{d}}\tilde{U}_m^{(i)}(x)}{\mathrm{d}x}\mathrm{d}x-\int_0^{L^{(i)}}\tilde{A}_n^{(i)}(x)\tilde{U}_m^{(i)}(x)\mathrm{d}x-\rho^{(i)}\omega_n^2\int_0^{L}\tilde{U}_n^{(i)}(x)\tilde{U}_m^{(i)}(x)\mathrm{d}x\end{aligned} \tag{26}$$

where $\tilde{S}_n^{(i)}$, $\tilde{M}_n^{(i)}$ and $\tilde{N}_n^{(i)}$ are shear force, bending moment and axial force of the nth mode. Taking into account Eq.(11) and Eq.(12) that define the vectors of nodal displacements and forces respectively, summing Eq.(25) and Eq.(26) yields

$$\left(\tilde{\mathbf{P}}_n^{(i,nod)}\right)^T \tilde{\mathbf{U}}_m^{(i,nod)} = \int_0^{L^{(i)}} \left(\frac{\overline{\mathrm{d}}^2 \tilde{\mathbf{U}}_n^{(i)}}{\mathrm{d}x^2}\right)^T \mathbf{K}^{(i)} \frac{\overline{\mathrm{d}}^2 \tilde{\mathbf{U}}_m^{(i)}}{\mathrm{d}x^2} \mathrm{d}x - \int_0^{L^{(i)}} \left(\tilde{\mathbf{F}}_n^{(i)}\right)^T \tilde{\mathbf{U}}_m^{(i)} \mathrm{d}x - \rho^{(i)} \omega_n^2 \int_0^{L^{(i)}} \left(\tilde{\mathbf{U}}_n^{(i)}\right)^T \tilde{\mathbf{U}}_m^{(i)} \mathrm{d}x \tag{27}$$

where, for the ith member

$$\tilde{\mathbf{U}}_m^{(i)}(x) = \begin{Bmatrix} \tilde{U}_m^{(i)}(x) \\ \tilde{V}_m^{(i)}(x) \end{Bmatrix}; \qquad \tilde{\mathbf{U}}_n^{(i)}(x) = \begin{Bmatrix} \tilde{U}_n^{(i)}(x) \\ \tilde{V}_n^{(i)}(x) \end{Bmatrix} \tag{28a,b}$$

$$\tilde{\mathbf{F}}_n^{(i)}(x) = \begin{Bmatrix} \tilde{A}_n^{(i)}(x) \\ \tilde{B}_n^{(i)}(x) \end{Bmatrix} \tag{29}$$

$$\mathbf{K}^{(i)} = \begin{bmatrix} EA^{(i)} & 0 \\ 0 & EI^{(i)} \end{bmatrix} \tag{30}$$

Next, be $\mathbf{P}_n^{(i,nod)}$ and $\mathbf{U}_m^{(i,nod)}$ the nodal forces and nodal displacements expressed in the global coordinate system, related to the corresponding $\tilde{\mathbf{P}}_n^{(i,nod)}$ and $\tilde{\mathbf{U}}_m^{(i,nod)}$ in the local coordinate system by the following well-known relations:

$$\tilde{\mathbf{P}}_n^{(i,nod)} = \mathbf{T}^{(i)} \mathbf{P}_n^{(i,nod)} \qquad \tilde{\mathbf{U}}_m^{(i,nod)} = \mathbf{T}^{(i)} \mathbf{U}_m^{(i,nod)} \tag{31a,b}$$

being $\mathbf{T}^{(i)}$ the transformation matrix in Eqs.(17). From Eqs.(31) it is readily seen that:

$$\left(\mathbf{P}_n^{(i,nod)}\right)^T \mathbf{U}_m^{(i,nod)} = \left(\tilde{\mathbf{P}}_n^{(i,nod)}\right)^T \tilde{\mathbf{U}}_m^{(i,nod)} \tag{32}$$

The term on the l.h.s. of Eq.(32) represents the work done, in the ith member, by the nodal forces of mode n for the nodal displacements of mode m, expressed in the global coordinate system. Because the nodal forces of mode n are in equilibrium, the total work over all elements of the plane structure, computed for the set of nodal displacements associated with mode m, is equal to zero if no mass-spring subsystems are applied at member-to-member nodes. Therefore, summing up terms on the l.h.s. of Eq.(32) for i=1,2,…Ne yields

$$\sum_{i=1}^{Ne}\left(\mathbf{P}_n^{(i,nod)}\right)^T \mathbf{U}_m^{(i,nod)} = 0 \tag{33}$$

Based on Eq.(33), Eq.(32) and Eq.(27) it can be stated that

$$\begin{aligned}\sum_{i=1}^{Ne}\int_0^{L^{(i)}}\left(\frac{\overline{\mathrm{d}}^2\tilde{\mathbf{U}}_n^{(i)}}{\mathrm{d}x^2}\right)^T \mathbf{K}^{(i)}\frac{\overline{\mathrm{d}}^2\tilde{\mathbf{U}}_m^{(i)}}{\mathrm{d}x^2}\mathrm{d}x - \sum_{i=1}^{Ne}\int_0^{L^{(i)}}\left(\tilde{\mathbf{F}}_n^{(i)}\right)^T \tilde{\mathbf{U}}_m^{(i)}\mathrm{d}x - \\ -\omega_n^2\sum_{i=1}^{Ne}\rho^{(i)}\int_0^{L^{(i)}}\left(\tilde{\mathbf{U}}_n^{(i)}\right)^T \tilde{\mathbf{U}}_m^{(i)}\mathrm{d}x = 0\end{aligned} \tag{34}$$

Recognize that, in Eq.(34), inertia forces are treated as body forces according to D'Alembert principle [48]. The procedure above may be repeated starting from Eq.(21) for $\tilde{V}_m^{(i)}(x)$ and Eq.(22) for $\tilde{U}_m^{(i)}(x)$ of the mth mode, to be multiplied respectively by deflection $\tilde{V}_n^{(i)}(x)$ and axial displacement $\tilde{U}_n^{(i)}(x)$ of the nth mode, to derive:

$$\begin{aligned}\sum_{i=1}^{Ne}\int_0^{L^{(i)}}\left(\frac{\overline{\mathrm{d}}^2\tilde{\mathbf{U}}_m^{(i)}}{\mathrm{d}x^2}\right)^T \mathbf{K}^{(i)}\frac{\overline{\mathrm{d}}^2\tilde{\mathbf{U}}_n^{(i)}}{\mathrm{d}x^2}\mathrm{d}x - \sum_{i=1}^{Ne}\int_0^{L^{(i)}}\left(\tilde{\mathbf{F}}_m^{(i)}\right)^T \tilde{\mathbf{U}}_n^{(i)}\mathrm{d}x - \\ -\omega_m^2\sum_{i=1}^{Ne}\rho^{(i)}\int_0^{L^{(i)}}\left(\tilde{\mathbf{U}}_m^{(i)}\right)^T \tilde{\mathbf{U}}_n^{(i)}\mathrm{d}x = 0\end{aligned} \tag{35}$$

Eqs.(34)-(35) are the basis to derive orthogonality conditions for the modes, as follows.

The first orthogonality condition is built from the difference between Eq.(34) and Eq.(35):

$$\left(\omega_m^2-\omega_n^2\right)\sum_{i=1}^{Ne}\rho^{(i)}\int_0^{L^{(i)}}\left(\tilde{\mathbf{U}}_m^{(i)}\right)^T \tilde{\mathbf{U}}_n^{(i)}\mathrm{d}x + Q\left(\omega_m,\omega_n\right) = 0 \tag{36}$$

where $Q(\omega_m,\omega_n)$ is given as

$$Q=\sum_{i=1}^{Ne}\sum_{j=1}^{N^{(i)}}\left(\tilde{\mathbf{U}}_m^{(i)}\left(x_j^{(i)}\right)\right)^T\left(\mathbf{K}_{AB}^{(i)}(\omega_n)-\mathbf{K}_{AB}^{(i)}(\omega_m)\right)\tilde{\mathbf{U}}_n^{(i)}\left(x_j^{(i)}\right) \tag{37}$$

for

$$\mathbf{K}_{AB}^{(i)}(\omega)=\begin{bmatrix}\kappa_{A_j}^{(i)}(\omega) & 0\\ 0 & \kappa_{B_j}^{(i)}(\omega)\end{bmatrix} \tag{38}$$

with $\kappa_{A_j}^{(i)}(\omega)$ and $\kappa_{B_j}^{(i)}(\omega)$ frequency-dependent stiffness given as Eq.(5).

The second orthogonality condition is obtained subtracting Eq.(35), as multiplied by ω_n, from Eq.(34) as multiplied by ω_m, i.e.:

$$\begin{aligned}&(\omega_m-\omega_n)\sum_{i=1}^{Ne}\int_0^{L^{(i)}}\left(\frac{\bar{\mathrm{d}}^2\tilde{\mathbf{U}}_m^{(i)}}{\mathrm{d}x^2}\right)^T\mathbf{K}^{(i)}\frac{\bar{\mathrm{d}}^2\tilde{\mathbf{U}}_n^{(i)}}{\mathrm{d}x^2}\mathrm{d}x+\\&+\omega_m\omega_n(\omega_m-\omega_n)\sum_{i=1}^{Ne}\rho^{(i)}\int_0^{L^{(i)}}\left(\tilde{\mathbf{U}}_m^{(i)}\right)^T\tilde{\mathbf{U}}_n^{(i)}\mathrm{d}x+Z(\omega_m,\omega_n)=0\end{aligned} \tag{39}$$

where $Z(\omega_m,\omega_n)$ is given as

$$\begin{aligned}Z=&\sum_{i=1}^{Ne}\sum_{j=1}^{N^{(i)}}\left(\tilde{\mathbf{U}}_m^{(i)}\left(x_j^{(i)}\right)\right)^T\left(\omega_m\mathbf{K}_{AB}^{(i)}(\omega_n)-\omega_n\mathbf{K}_{AB}^{(i)}(\omega_m)\right)\tilde{\mathbf{U}}_n^{(i)}\left(x_j^{(i)}\right)+\\&(\omega_n-\omega_m)\sum_{i=1}^{Ne}\sum_{j=1}^{N^{(i)}}\frac{\tilde{M}_n^{(i)}(x_j)}{k_{\Delta\Theta_j}^{(i)}}\left(\tilde{M}_m^{(i)}(x_j)+\frac{EI^{(i)}}{k_{\Delta\Theta_j}^{(i)}}\int_0^{L^{(i)}}\tilde{M}_m^{(i)}(x_j)\delta\left(x-x_j^{(i)}\right)\delta\left(x-x_j^{(i)}\right)\mathrm{d}x\right)\end{aligned} \tag{40}$$

Recognize that Eq.(36) and Eq.(39) are derived on integrating by parts the integral terms involving $\tilde{\mathbf{F}}_n^{(i)}$ in Eq.(34), $\tilde{\mathbf{F}}_m^{(i)}$ in Eq.(35) and expressing the 2nd derivatives $\bar{\mathrm{d}}^2V_m/\mathrm{d}x^2$, $\bar{\mathrm{d}}^2V_n/\mathrm{d}x^2$ using the beam equations, see Eqs.(A.6) in Appendix A.

The orthogonality conditions given by Eqs.(36)-(39) have been derived on the assumption that no external mass-spring subsystems are present at member-to-member nodes, see Eq.(33) for equilibrium. This case, however, can readily be treated within the same framework. Assuming indeed that the mass-spring subsystem at node N_k acts along an arbitrary direction $\mathbf{t}^{(N_k)} = \left\{ t_X^{(N_k)} \quad t_Y^{(N_k)} \right\}^T$, $\left\| \mathbf{t}^{(N_k)} \right\| = 1$ in the global coordinate system, Eq.(33) changes as

$$\sum_{i=1}^{Ne} \left(\mathbf{P}_n^{(i,nod)} \right)^T \mathbf{U}_m^{(i,nod)} = \sum_{N_k} \left(\mathbf{R}_n^{(N_k)} \right)^T \mathbf{U}_m^{(N_k)} \tag{41}$$

where

$$\mathbf{R}_n^{(N_k)} = -\kappa^{(N_k)} \left(\omega_n \right) \mathbf{t}^T \mathbf{U}_n^{(N_k)} \mathbf{t} = -\mathbf{K}^{(N_k)} \left(\omega_n \right) \mathbf{U}_n^{(N_k)} \tag{42}$$

with $\mathbf{K}^{(N_k)}(\omega)$ given by Eq.(20), while $\mathbf{U}_n^{(N_k)}$ is the vector of displacements of the node in the global coordinate system; obviously, $\mathbf{U}_n^{(N_k)} = \mathbf{U}_n^{(i)}$ for any i^{th} member connected to the node N_k. Starting from Eq.(41), it is readily seen that the orthogonality conditions hold the form of Eqs.(36)-(39) except for terms Q, Z, to be replaced by Q' and Z' given as

$$Q' = Q + \sum_{N_k} \left(\mathbf{U}_m^{(N_k)} \right)^T \left(\mathbf{K}^{(N_k)} \left(\omega_n \right) - \mathbf{K}^{(N_k)} \left(\omega_m \right) \right) \mathbf{U}_n^{(N_k)} \tag{43}$$

$$Z' = Z + \sum_{N_k} \left(\mathbf{U}_m^{(N_k)} \right)^T \left(\omega_m \mathbf{K}^{(N_k)} \left(\omega_n \right) - \omega_n \mathbf{K}^{(N_k)} \left(\omega_m \right) \right) \mathbf{U}_n^{(N_k)} \tag{44}$$

It is noteworthy that the orthogonality conditions given by Eqs.(36)-(39) represent a generalization to the plane structure in Figure 1 of the orthogonality conditions derived in ref. [49] for a beam with end viscous dampers.

5. EXACT MODAL SOLUTION

The final step of the study is to derive the exact modal response to arbitrary loading. For this the orthogonality conditions obtained in Section 4 will be used, as explained in the following.

5.1. Modal impulse and frequency response functions

First, bending and axial motion equations of the ith member under impulsive loading are written in the local coordinate system of the member:

$$EI^{(i)}\frac{\overline{\partial}^4\tilde{v}^{(i)}(x,t)}{\partial x^4}-\tilde{b}^{(i)}(x,t)+\rho^{(i)}\ddot{\tilde{v}}^{(i)}(x,t)-\tilde{q}_y^{(i)}(x)\delta(t)=0 \tag{45}$$

$$EA^{(i)}\frac{\overline{\partial}^2\tilde{u}^{(i)}(x,t)}{\partial x^2}+\tilde{a}^{(i)}(x,t)-\rho^{(i)}\ddot{\tilde{u}}^{(i)}(x,t)+\tilde{q}_x^{(i)}(x)\delta(t)=0 \tag{46}$$

In Eqs.(45)-(46), $\tilde{q}_y^{(i)}(x)\delta(t)$ and $\tilde{q}_x^{(i)}(x)\delta(t)$ are space-dependent impulsive loads at t=0, with $\tilde{q}_y^{(i)}(x)$ and $\tilde{q}_x^{(i)}(x)$ governing the space distribution over the ith member, see Figure 2. Further, $\tilde{b}^{(i)}(x,t)$ and $\tilde{a}^{(i)}(x,t)$ are the time-dependent generalised functions associated with the mass-spring subsystems and joints, i.e.

$$\tilde{b}^{(i)}(x,t)=\sum_{j=1}^{N^{(i)}}\tilde{r}_{B_j}^{(i)}(t)\delta\left(x-x_j^{(i)}\right)+EI^{(i)}\Delta\tilde{\theta}_j^{(i)}(t)\delta^{(2)}\left(x-x_j^{(i)}\right) \tag{47}$$

$$\tilde{a}^{(i)}(x,t)=\sum_{j=1}^{N^{(i)}}\tilde{r}_{A_j}^{(i)}(t)\delta\left(x-x_j^{(i)}\right) \tag{48}$$

In Eqs.(47)-(48), $\Delta\tilde{\theta}_j^{(i)}(t)$ denotes the relative rotation between adjacent cross sections at $x=x_j^{(i)}$

$$\Delta\tilde{\theta}_j^{(i)}(t)=-\left(k_{\Delta\Theta_j}^{(i)}\right)^{-1}\tilde{m}\left(x_j^{(i)},t\right) \tag{49}$$

where $\tilde{m}\left(x_j^{(i)},t\right)$ is the bending moment, while symbols $\tilde{r}_{B_j}^{(i)}(t)$ and $\tilde{r}_{A_j}^{(i)}(t)$ denote the point forces exerted at $x=x_j^{(i)}$ by the mass-spring subsystem

$$\tilde{r}_{B_j}^{(i)}(t)=-k_{B_j}^{(i)}\left(\tilde{v}^{(i)}\left(x_j^{(i)},t\right)-\tilde{z}_{B_j,1}^{(i)}(t)\right)-M_{B_j,0}^{(i)}\ddot{\tilde{v}}^{(i)}\left(x_j^{(i)},t\right) \tag{50}$$

$$\tilde{r}_{A_j}^{(i)}(t) = -k_{A_j}^{(i)}\left(\tilde{u}^{(i)}\left(x_j^{(i)},t\right) - \tilde{z}_{A_j,1}^{(i)}(t)\right) - M_{A_j,0}^{(i)}\ddot{\tilde{u}}^{(i)}\left(x_j^{(i)},t\right) \tag{51}$$

In Eqs.(50)-(51), $\tilde{z}_{B_j,1}^{(i)}(t)$ and $\tilde{z}_{A_j,1}^{(i)}(t)$ are the displacements of mass $M_{B_j,1}^{(i)}$ and mass $M_{A_j,1}^{(i)}$ of the mass-spring subsystems, while the mass-dependent terms are the inertia forces acting on masses $M_{B_j,0}^{(i)}$ and $M_{A_j,0}^{(i)}$ attached to the beam (see Figure 2).

According to the modal superposition principle, the following expressions can be adopted in the ith member

$$\tilde{\mathbf{u}}^{(i)}(x,t) = \begin{Bmatrix} \tilde{u}^{(i)}(x,t) \\ \tilde{v}^{(i)}(x,t) \end{Bmatrix} = \sum_{n=1}^{\infty} c_n(t)\tilde{\mathbf{U}}_n^{(i)}(x) \tag{52}$$

$$\tilde{\mathbf{f}}^{(i)}(x,t) = \sum_{n=1}^{\infty} c_n(t)\begin{Bmatrix} \tilde{A}_n^{(i)}(x) \\ \tilde{B}_n^{(i)}(x) \end{Bmatrix} = \sum_{n=1}^{\infty} c_n(t)\tilde{\mathbf{F}}_n^{(i)}(x) \tag{53}$$

with $\tilde{\mathbf{U}}_n^{(i)}(x)$ and $\tilde{\mathbf{F}}_n^{(i)}(x)$ given by Eq.(28b) and Eq.(29). Also, due to the impulsive nature of the loading, it can be written that [49,50]

$$c_n(t) = \gamma_n \mathrm{e}^{\mathrm{i}\omega_n t}, \qquad c_n(t) = \gamma_n^* \mathrm{e}^{-\mathrm{i}\omega_n t} \tag{54a,b}$$

where γ_n and γ_n^* are a complex conjugate pair.

First, assume that $c_n(t)$ is given as Eq.(54a), that is $c_n(t) = \gamma_n \mathrm{e}^{\mathrm{i}\omega_n t}$. Replace Eq.(52) for $\tilde{v}^{(i)}(x,t)$ and $\tilde{u}^{(i)}(x,t)$ in Eqs.(45)-(46), multiply Eq.(45) by $\tilde{V}_m^{(i)}(x)$ and Eq.(46) by $\tilde{U}_m^{(i)}(x)$, and integrate over the length $L^{(i)}$ of the ith member. On integrating by parts the integrals involving the 4th derivative in Eq.(45) and 2nd derivative in Eq.(46), summing Eq.(45) and Eq.(46) yields

$$\left(\tilde{\mathbf{p}}^{(i,nod)}\right)^T \tilde{\mathbf{U}}_m^{(i,nod)} = \int_0^{L^{(i)}} \left(\frac{\overline{\mathrm{d}}^2 \tilde{\mathbf{u}}^{(i)}}{\mathrm{d}x^2}\right)^T \mathbf{K}^{(i)} \frac{\overline{\mathrm{d}}^2 \tilde{\mathbf{U}}_m^{(i)}}{\mathrm{d}x^2} \mathrm{d}x - \int_0^{L^{(i)}} \left(\tilde{\mathbf{f}}^{(i)}\right)^T \tilde{\mathbf{U}}_m^{(i)} \mathrm{d}x + \int_0^{L^{(i)}} \rho^{(i)} \left(\ddot{\tilde{\mathbf{u}}}^{(i)}\right)^T \tilde{\mathbf{U}}_m^{(i)} \mathrm{d}x - \int_0^{L^{(i)}} \left(\tilde{\mathbf{q}}^{(i)}\right)^T \tilde{\mathbf{U}}_m^{(i)} \mathrm{d}x \tag{55}$$

where $\tilde{\mathbf{q}}^{(i)} = \left\{\tilde{q}_x^{(i)} \quad \tilde{q}_y^{(i)}\right\}^T$ is the vector collecting the space-dependent loading functions, $\tilde{\mathbf{U}}_m^{(i,nod)}$ is the vector of nodal displacements Eq.(12) of the mth mode, while vector $\tilde{\mathbf{p}}^{(i,nod)}$ represents the vector of nodal forces of the ith member in local coordinate system, as expressed by the modal expansion, i.e.

$$\tilde{\mathbf{p}}^{(i,nod)} = \sum_{n=1}^{\infty} c_n(t) \tilde{\mathbf{P}}_n^{(i,nod)} \tag{56}$$

being $\tilde{\mathbf{P}}_n^{(i,nod)}$ the vector of nodal forces Eq.(11) of the nth mode.

Now, denoting by $\mathbf{p}^{(i,nod)}$ the vector of nodal forces of the ith member in the global coordinate system, the following relation can be written for nodal forces/displacements in local and global coordinate system (see corresponding Eq.(32) in Section 4)

$$\left(\mathbf{p}^{(i,nod)}\right)^T \mathbf{U}_m^{(i,nod)} = \left(\tilde{\mathbf{p}}^{(i,nod)}\right)^T \tilde{\mathbf{U}}_m^{(i,nod)} \tag{57}$$

Assuming that neither impulsive forces nor external mass-spring subsystems are applied at the nodes, for equilibrium it can be written that

$$\sum_{i=1}^{Ne} \left(\mathbf{p}^{(i,nod)}\right)^T \mathbf{U}_m^{(i,nod)} = 0 \tag{58}$$

Eq.(58), Eq.(57) and Eq.(55) yield

$$\sum_{i=1}^{Ne}\int_0^{L^{(i)}}\left(\frac{\overline{\mathrm{d}}^2\tilde{\mathbf{u}}^{(i)}}{\mathrm{d}x^2}\right)^T\mathbf{K}^{(i)}\frac{\overline{\mathrm{d}}^2\tilde{\mathbf{U}}_m^{(i)}}{\mathrm{d}x^2}\mathrm{d}x-\sum_{i=1}^{Ne}\int_0^{L^{(i)}}\left(\tilde{\mathbf{f}}^{(i)}\right)^T\tilde{\mathbf{U}}_m^{(i)}\mathrm{d}x+$$
$$+\sum_{i=1}^{Ne}\rho^{(i)}\int_0^{L^{(i)}}\left(\ddot{\tilde{\mathbf{u}}}^{(i)}\right)^T\tilde{\mathbf{U}}_m^{(i)}\mathrm{d}x=\sum_{i=1}^{Ne}\int_0^{L^{(i)}}\left(\tilde{\mathbf{q}}^{(i)}\right)^T\tilde{\mathbf{U}}_m^{(i)}\mathrm{d}x \tag{59}$$

To further manipulate Eq.(59), consider Eq.(53) for $\tilde{\mathbf{f}}^{(i)}(x,t)$ and Eq.(52) for $\ddot{\tilde{\mathbf{u}}}^{(i)}(x,t)$, where

$$\ddot{c}_n(t)=-\omega_n^2c_n(t) \tag{60}$$

being $c_n(t)=\gamma_n\mathrm{e}^{\mathrm{i}\omega_n t}$, see Eq.(54a). Then, on integrating by parts the integral term involving $\tilde{\mathbf{f}}^{(i)}$ on the l.h.s. of Eq.(59) and using the second orthogonality condition Eq.(39), the following equation can be obtained in $\ddot{c}_n(t)$:

$$\sum_{n=1}^{\infty}\frac{\ddot{c}_n}{\omega_n^2}\cdot\left(\sum_{i=1}^{Ne}\sum_{j=1}^{N^{(i)}}\frac{\omega_n}{(\omega_m-\omega_n)}\left(\tilde{\mathbf{U}}_m^{(i)}(x_j)\right)^T\left(\mathbf{K}_{AB}(\omega_n)-\mathbf{K}_{AB}(\omega_m)\right)\tilde{\mathbf{U}}_n^{(i)}(x_j)\right.$$
$$\left.+\rho^{(i)}\left(\omega_m\omega_n+\omega_n^2\right)\int_0^{L^{(i)}}\left(\tilde{\mathbf{U}}_m^{(i)}\right)^T\tilde{\mathbf{U}}_n^{(i)}\mathrm{d}x\right)=\eta_m\delta(t) \tag{61}$$

where

$$\eta_m=\sum_{i=1}^{Ne}\int_0^{L^{(i)}}\left(\tilde{\mathbf{q}}^{(i)}\right)^T\tilde{\mathbf{U}}_m^{(i)}\mathrm{d}x \tag{62}$$

Being $\tilde{\mathbf{q}}^{(i)}=\left\{\tilde{q}_x^{(i)}\quad\tilde{q}_y^{(i)}\right\}^T$ the vector collecting the space-dependent loading functions and in view of Eq.(28a) for $\tilde{\mathbf{U}}_m^{(i)}$, η_m in Eq.(62) is the projection of the space-dependent functions $\tilde{q}_y^{(i)}(x)$, $\tilde{q}_x^{(i)}(x)$ of the impulsive loadings on the deflection/axial-displacement eigenfunctions $\tilde{V}_m^{(i)}(x)$, $\tilde{U}_m^{(i)}(x)$ of the mth mode, along every member of the plane structure.

Next, attention is focused on the expression within parenthesis in Eq.(61), which multiplies $\ddot{c}_n/\omega_n^2$ for n=1,…∞. In view of the first orthogonality condition given by Eq.(36), the expression is

equal to zero for $\omega_n \neq \omega_m$. On the other hand, for $\omega_n = \omega_m$ the second term of the expression is equal to $2\rho^{(i)}\omega_m^2 \int_0^{L^{(i)}} \left(\tilde{\mathbf{U}}_m^{(i)}\right)^T \tilde{\mathbf{U}}_m^{(i)} \mathrm{d}x$, while the following limit provides the first term:

$$\lim_{\omega_n \to \omega_m} \frac{\omega_n \left(\tilde{\mathbf{U}}_m^{(i)}\left(x_j\right)\right)^T \left(\mathbf{K}_{AB}^{(i)}\left(\omega_n\right) - \mathbf{K}_{AB}^{(i)}\left(\omega_m\right)\right) \tilde{\mathbf{U}}_n^{(i)}\left(x_j\right)}{\left(\omega_m - \omega_n\right)} = \left(\tilde{\mathbf{U}}_m^{(i)}\left(x_j\right)\right)^T \mathbf{E}_{AB}^{(i)}\left(\omega_m\right) \tilde{\mathbf{U}}_m^{(i)}\left(x_j\right) \tag{63}$$

In Eq.(63), $\mathbf{E}_{AB}^{(i)}\left(\omega\right)$ is the 2×2 matrix

$$\mathbf{E}_{AB}^{(i)}\left(\omega\right) = \begin{bmatrix} e_{A_j}^{(i)}\left(\omega\right) & 0 \\ 0 & e_{B_j}^{(i)}\left(\omega\right) \end{bmatrix} \tag{64}$$

where $e_{B_j}^{(i)}\left(\omega\right)$ and $e_{A_j}^{(i)}\left(\omega\right)$ denote frequency-dependent terms with the same analytical form, as indeed $\kappa_{A_j}^{(i)}\left(\omega\right)$ and $\kappa_{B_j}^{(i)}\left(\omega\right)$ in Eq.(38) for $\mathbf{K}_{AB}^{(i)}\left(\omega\right)$ have the same expression for the mass-spring subsystems acting in transverse and axial directions, see Eq.(5). Specifically, $e_{B_j}^{(i)}\left(\omega_m\right)$ is obtained as

$$e_{B_j}^{(i)}\left(\omega_m\right) = \lim_{\omega_n \to \omega_m} \omega_n \frac{\kappa_{B_j}^{(i)}\left(\omega_n\right) - \kappa_{B_j}^{(i)}\left(\omega_m\right)}{\left(\omega_m - \omega_n\right)} = 2M_{B_{j,0}}^{(i)}\omega_m^2 + \frac{f_{B_j}^{(i)}}{g_{B_j}^{(i)}}\omega_m^2 \tag{65}$$

with

$$f_{B_j}^{(i)} = 2\left(k_{B_{j,1}}^{(i)}\right)^2 \left(\left(k_{B_{j,2}}^{(i)} + k_{B_{j,3}}^{(i)}\right)^2 M_{B_{j,1}}^{(i)} + \left(\left(k_{B_{j,2}}^{(i)}\right)^2 - 2\omega_m^2\left(k_{B_{j,2}}^{(i)} + k_{B_{j,3}}^{(i)}\right)M_{B_{j,1}}^{(i)}\right)M_{B_{j,2}}^{(i)} + \omega_m^4 M_{B_{j,1}}^{(i)}\left(M_{B_{j,2}}^{(i)}\right)^2\right) \tag{66}$$

$$g_{B_j}^{(i)} = \left(k_{B_{j,1}}^{(i)}\left(k_{B_{j,2}}^{(i)} + k_{B_{j,3}}^{(i)} - \omega_m^2 M_{B_{j,2}}^{(i)}\right) + \omega_m^2 M_{B_{j,1}}^{(i)}\left(\omega_m^2 M_{B_{j,2}}^{(i)} - k_{B_{j,3}}^{(i)}\right) + k_{B_{j,2}}^{(i)}\left(k_{B_{j,3}}^{(i)} - \omega_m^2\left(M_{B_{j,1}}^{(i)} + M_{B_{j,2}}^{(i)}\right)\right)\right)^2 \tag{67}$$

On the other hand, $e_{A_j}^{(i)}\left(\omega\right)$ is obtained from Eq.(65) on replacing $k_{B_{j,k}}^{(i)}$ with $k_{A_{j,k}}^{(i)}$ and $M_{B_{j,k}}^{(i)}$ with $M_{A_{j,k}}^{(i)}$ in Eqs.(66)-(67).

Based on Eq.(63), for $\omega_m = \omega_n$ the following uncoupled differential equations can finally be obtained in $\ddot{c}_m\left(t\right)$:

$$\ddot{c}_m \Pi_m = \eta_m \delta(t) \tag{68}$$

where Π_m is given as

$$\Pi_m = \sum_{i=1}^{Ne} \sum_{j=1}^{N^{(i)}} \left(\omega_m^{-2} \left(\tilde{\mathbf{U}}_m^{(i)}(x_j) \right)^T \mathbf{E}_{AB}^{(i)}(\omega_m) \tilde{\mathbf{U}}_m^{(i)}(x_j) + \sum_{i=1}^{Ne} 2\rho^{(i)} \int_0^{L^{(i)}} \left(\tilde{\mathbf{U}}_m^{(i)} \right)^T \tilde{\mathbf{U}}_m^{(i)} \mathrm{d}x \right) \tag{69}$$

That is, Π_m depends on the continuous mass distribution (second term in Eq.(69)) as well as on the mass-stiffness parameters of the discrete mass-spring subsystems along every member.

Eq.(68) is the basis to derive the complex coefficients in Eq.(54a), following the approach previously applied in ref. [49]. Indeed, integrating Eq.(68) over the time domain yields $\dot{c}_m(0^+) = (\Pi_m)^{-1} \eta_m$, and taking into account that $\dot{c}_m = \mathrm{i}\omega_m c_m$ in view of Eq.(54a), the following relation can be obtained for γ_m:

$$\gamma_m = \frac{\eta_m}{\mathrm{i}\omega_m \Pi_m} \tag{70}$$

At this stage, the procedure above shall be repeated assuming that, for every mode n, $c_n(t)$ in Eqs.(52)-(53)-(56) is $c_n(t) = \gamma_n^* \mathrm{e}^{-\mathrm{i}\omega_n t}$ with γ_n^* complex conjugate of γ_n, see Eq.(54b). As a result, the impulse response function of the mth mode is finally derived in the following form:

$$h_m(t) = \gamma_m \mathrm{e}^{\mathrm{i}\omega_m t} + \gamma_m^* \mathrm{e}^{-\mathrm{i}\omega_m t} = \frac{2\eta_m}{\omega_m \Pi_m} \sin(\omega_m t) \tag{71}$$

where $\mathrm{e}^{\pm \mathrm{i}\omega_m t} = \cos(\omega_m t) \pm \mathrm{i} \sin(\omega_m t)$ according to Euler's formula. From Eq.(71), it is evident that the equation governing the impulse response function of every mode is the following 2nd order differential equation

$$\ddot{h}_m(t) + \omega_m^2 h_m(t) = \frac{2\eta_m}{\Pi_m} \delta(t) \tag{72}$$

Obviously, under the assumption of proportional damping Eq.(72) will take the following form:

$$\ddot{h}_m(t)+2\zeta_m\omega_m\dot{h}_m(t)+\omega_m^2 h_m(t)=\frac{2\eta_m}{\Pi_m}\delta(t) \tag{73}$$

with the associated modal impulse response function and modal frequency response function, for modal damping ratio $\zeta_m<1$:

$$h_m(t)=\frac{2\eta_m}{\omega_{Dm}\Pi_m}\mathrm{e}^{-\zeta_m\omega_m t}\sin(\omega_{Dm}t) \qquad \omega_{Dm}=\omega_m\sqrt{1-\zeta_m^2} \tag{74a,b}$$

$$H_m(\omega)=\frac{2\eta_m}{\Pi_m}\cdot\frac{1}{\omega_m^2-\omega^2+\mathrm{i}(2\zeta_m\omega_m\omega)} \tag{75}$$

The formulation above can readily be updated whereas impulsive forces or external mass-spring subsystems are present at member-to-member nodes. In these cases, Eq.(58) reads

$$\sum_{i=1}^{Ne}\left(\mathbf{p}^{(i,nod)}\right)^T\mathbf{U}_m^{(i,nod)}=\sum_{N_k}\left(\mathbf{r}^{(N_k)}\right)^T\mathbf{U}_m^{(i,nod)}+\sum_{N_k}\left(\mathbf{f}^{(N_k)}\right)^T\mathbf{U}_m^{(i,nod)} \tag{76}$$

where $\mathbf{r}^{(N_k)}$ and $\mathbf{f}^{(N_k)}$ are reaction forces of the nodal mass-spring subsystems and nodal impulsive forces. Taking into account the orthogonality conditions given by Eqs.(36)-(39) with Q and Z replaced by Q' and Z', it can readily be demonstrated that the impulse response function of the mth mode holds the form of Eq.(74a) (or Eq.(71) with no damping), where η_m and Π_m are modified as

$$\eta_m=\sum_{i=1}^{Ne}\int_0^{L^{(i)}}\left(\tilde{\mathbf{q}}^{(i)}\right)^T\tilde{\mathbf{U}}_m^{(i)}dx+\sum_{N_k}\left(\mathbf{f}^{(N_k)}\right)^T\mathbf{U}_m^{(i,nod)} \tag{77}$$

$$\begin{aligned}\Pi_m=&\sum_{i=1}^{Ne}\sum_{j=1}^{N^{(i)}}\left(\omega_m^{-2}\left(\tilde{\mathbf{U}}_m^{(i)}(x_j)\right)^T\mathbf{E}_{AB}^{(i)}(\omega_m)\tilde{\mathbf{U}}_m^{(i)}(x_j)+\sum_{i=1}^{Ne}2\rho^{(i)}\int_0^{L^{(i)}}\left(\tilde{\mathbf{U}}_m^{(i)}\right)^T\tilde{\mathbf{U}}_n^{(i)}\mathrm{d}x\right)+\\&+\sum_{N_k}\omega_m^{-2}\left(\mathbf{U}_m^{(N_k)}\right)^T\mathbf{E}^{(N_k)}(\omega_m)\mathbf{U}_m^{(N_k)}\end{aligned} \tag{78}$$

In Eq.(78),

$$\mathbf{E}^{(N_k)}(\omega)=e^{(N_k)}(\omega)\begin{bmatrix} t_X^{(N_k)}t_X^{(N_k)} & t_X^{(N_k)}t_Y^{(N_k)} \\ t_X^{(N_k)}t_Y^{(N_k)} & t_Y^{(N_k)}t_Y^{(N_k)} \end{bmatrix} \tag{79}$$

where $e^{(N_k)}(\omega)$ is given as Eq.(65).

5.2. Response to arbitrary loading

Finally, Eq.(74a) and Eq.(75) can be used to compute the dynamic response of the plane structure in Figure 1 to arbitrary loads, with any space-distribution along the members.

Consider an arbitrary loading $q_x^{(i)}(x)f(t)$, $q_y^{(i)}(x)f(t)$ for i=1,2,…Ne, with $q_y^{(i)}(x)$ and $q_x^{(i)}(x)$ governing space dependence in the ith member. Be $\tilde{\mathbf{y}}^{(i)}(x,t)=\left\{u^{(i)} \quad v^{(i)} \quad \theta^{(i)} \quad n^{(i)} \quad m^{(i)} \quad s^{(i)} \quad z_{M_{A_{j,1}}}^{(i)} \quad ... \quad z_{M_{B_{j,1}}}^{(i)} \quad ...\right\}^T$ the vector collecting the time-dependent response variables in the ith member, including deflection/axial-displacements $z_{M_{A_{j,k}}}^{(i)}$, $z_{M_{B_{j,k}}}^{(i)}$ of the masses in the mass-spring subsystems. In view of Eq.(52), $\tilde{\mathbf{y}}^{(i)}(x,t)$ can be computed as:

$$\tilde{\mathbf{y}}^{(i)}(x,t)=\left(\sum_{m=1}^{\infty}\int_0^t h_m(t-\tau)f(\tau)d\tau\right)\tilde{\mathbf{Y}}_m^{(i)}(x) \tag{80}$$

where $\tilde{\mathbf{Y}}_m^{(i)}(x)=\left\{\tilde{U}_m^{(i)} \quad \tilde{V}_m^{(i)} \quad \tilde{\Theta}_m^{(i)} \quad \tilde{N}_m^{(i)} \quad \tilde{M}_m^{(i)} \quad \tilde{S}_m^{(i)} \quad \left(\tilde{Z}_{M_{A_{j,1}}}^{(i)}\right)_m \quad ... \quad \left(\tilde{Z}_{M_{B_{j,1}}}^{(i)}\right)_m \quad ...\right\}^T$ is the vector of eigenfunctions for the mth mode. Notice that Eq.(80) accounts for space-dependence of the loading function through the modal impulse response functions $h_m(t-\tau)$, Eq.(74a), which depend on the space-dependent functions $q_y^{(i)}(x)$ and $q_x^{(i)}(x)$ of the load through coefficient η_m, see Eq.(62).

Likewise, denoting by $\hat{\tilde{\mathbf{y}}}^{(i)}(x,\omega)$ and $\hat{f}(\omega)$ the Fourier Transforms of $\tilde{\mathbf{y}}^{(i)}(x,t)$ and $f(t)$ respectively,

$$\hat{\tilde{\mathbf{y}}}^{(i)}(x,\omega)=\sum_{m=1}^{\infty}H_m^{(i)}(\omega)\tilde{\mathbf{Y}}_m^{(i)}(x)\hat{f}(\omega) \tag{81}$$

$$\sum_{m=1}^{\infty}H_m^{(i)}(\omega)\tilde{\mathbf{Y}}_m^{(i)}(x)=\sum_{m=1}^{\infty}\mathbf{H}_m^{(i)}(x,\omega)=\mathbf{H}^{(i)}(x,\omega) \tag{82}$$

where $\mathbf{H}^{(i)}(x,\omega)$ denotes the vector of frequency response functions for all response variables in the ith member, i.e. $\mathbf{H}^{(i)}(x,\omega)=\left\{H_U^{(i)} \quad H_V^{(i)} \quad H_\Theta^{(i)} \quad H_N^{(i)} \quad H_M^{(i)} \quad H_S^{(i)} \quad H_{M_{A_{1,1}}}^{(i)} \quad \ldots \quad H_{M_{B_{1,1}}}^{(i)} \quad \ldots\right\}^T$.

5.3. Remarks

The proposed approach is an exact modal-superposition method for computing the dynamic response of the plane structure in Figure 1. Once the modal frequencies and undamped modes are determined from the global dynamic stiffness matrix and modal damping ratios are chosen, Eqs.(80)-(81)-(82) provide the time and frequency response variables in every member of the structure, including deflection/axial displacements of the masses in the mass-spring subsystems, see components of vector $\tilde{\mathbf{y}}^{(i)}(x,t)$ in Eq.(80), vectors $\hat{\tilde{\mathbf{y}}}^{(i)}(x,\omega)$ in Eq.(81) and $\mathbf{H}^{(i)}(x,\omega)$ in Eq.(82).

Eqs.(80)-(81)-(82) may also represent the exact benchmark solution for the modal response obtained by a FE procedure. Once modal damping ratios are built based on the common assumption that the damping matrix is proportional to mass and stiffness matrices (proportional Rayleigh damping [51]), Eqs.(80)-(81)-(82) will allow to check the accuracy of FE solutions with increasingly-refined meshes.

The proposed approach involves also computational advantages. The global dynamic stiffness matrix holds the same size if number/position of mass-spring subsystems and joints change. Also, time and frequency responses obtained from Eqs.(80)-(81)-(82) may readily be updated by changing only coefficient η_m if space-dependence/position of the load change. In contrast, a re-meshing would generally be required in the FE method, when number/position of mass-spring subsystem, joints and loads vary.

A further important remark is that the key step to obtain Eqs.(80)-(81)-(82) for time and frequency responses is the limit calculation in Eq.(65), which provides the analytical expression of matrix $\mathbf{E}_{AB}^{(i)}(\omega_m)$ to be considered in Eq.(69) for Π_m. It is evident that the procedure above can be generalised to any attached subsystem featuring a frequency-dependent stiffness $\kappa_{A_j}^{(i)}(\omega)$, $\kappa_{B_j}^{(i)}(\omega)$ for which the limit in Eq.(65) exists. Typical examples for which the limit exists are multi-mass-multi-spring subsystems, i.e. the so-called chains of oscillators [17,18]. Indeed, using the free-vibration equilibrium equations of the masses for every mode [17,18], it may be easily proved that the frequency-dependent stiffness of multi-mass-multi-spring subsystems with increasing number of masses and springs generally involves polynomial functions of the frequency ω (as Eq.(5) for the three-mass-three-spring subsystem), for which the limit in Eq.(65) can be computed in closed

analytical form. This makes it possible to generalise the exact modal analysis approach presented in this paper to continuous structures coupled with multi-mass-multi-spring subsystems.

6. NUMERICAL APPLICATION

Consider the plane structure in Figure 3 with mass-spring subsystems, rotational joints and springs, including a nodal spring applied at node N_3. For generality, various types of mass-spring subsystems and connections to the members are considered in the structure. The mass-spring subsystem in member 1 includes a single mass connected to the member by a spring in axial direction and a spring in transverse direction. The mass-spring subsystem in member 2 includes three masses and two springs; the springs act in transverse direction only, while it is assumed that masses and member have zero relative displacements in axial direction; that is, an attached total mass equal to the sum of the three masses will be considered for the axial vibrations of member 2. All system parameters are given in Table 1.

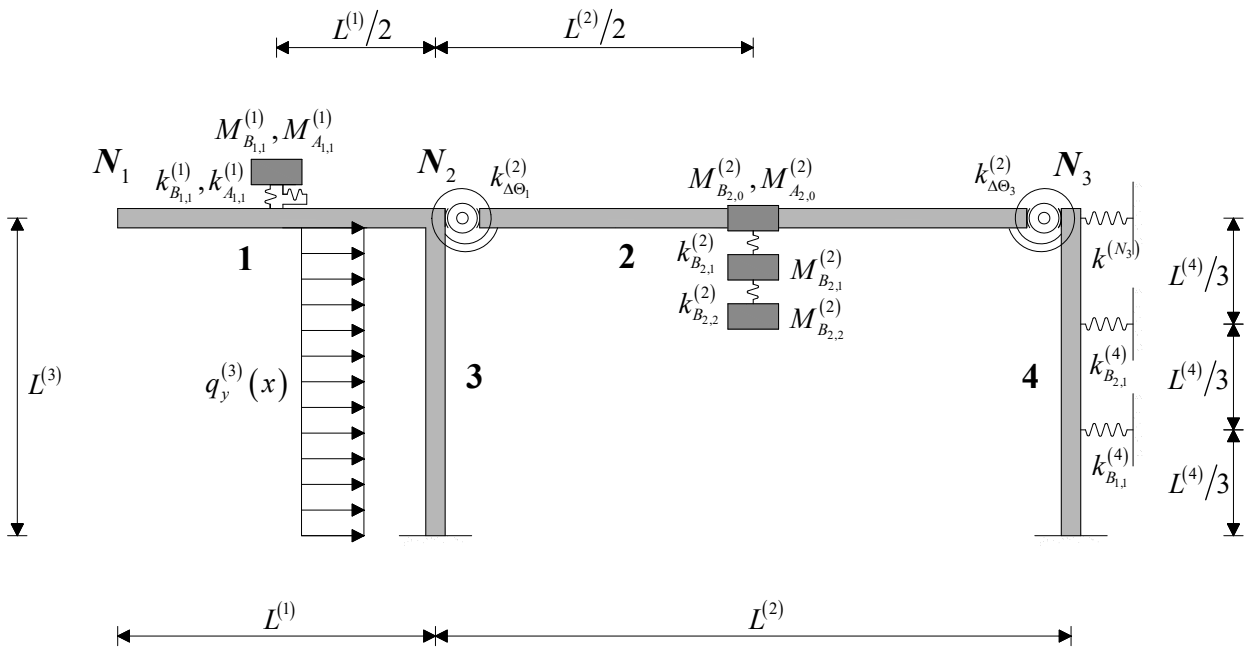

Figure 3. Plane structure with mass-spring subsystems, rotational joints and springs, under harmonic load uniformly distributed over member 3.

Table 1. Plane structure in Figure 3: parameters and number of elements for FE meshes in ADINA [53].

	Member 1	Member 2	Member 3	Member 4
$L^{(i)}$	3 m	6 m	3 m	3 m
$EI^{(i)}$	1.05495×10^{7} Nm^2	1.05495×10^{7} Nm^2	1.05495×10^{7} Nm^2	1.05495×10^{7} Nm^2
$EA^{(i)}$	1.25463×10^{9} N	1.25463×10^{9} N	1.25463×10^{9} N	1.25463×10^{9} N
$\rho^{(i)}$	49.54 kg/m	49.54 kg/m	49.54 kg/m	49.54 kg/m
Mass-spring	$k^{(1)}_{B_{1,1}}=5\times10^{5}$ Nm^{-1} $M^{(1)}_{B_{1,1}}=500$ kg $k^{(1)}_{A_{1,1}}=5\times10^{5}$ Nm^{-1} $M^{(1)}_{A_{1,1}}=500$ kg	$k^{(2)}_{B_{2,1}}=5\times10^{5}$ Nm^{-1} $k^{(2)}_{B_{2,2}}=5\times10^{5}$ Nm^{-1} $M^{(2)}_{B_{2,0}}=500$ kg $M^{(2)}_{B_{2,1}}=500$ kg $M^{(2)}_{B_{2,2}}=500$ kg $M^{(2)}_{A_{2,0}}=1500$ kg	-	-
Joint	-	$k^{(2)}_{\Delta\Theta_1}=5.27\times10^{7}$ Nm $k^{(2)}_{\Delta\Theta_3}=5.27\times10^{7}$ Nm	-	-
Spring	-	-	-	$k^{(4)}_{B_{1,1}}=5\times10^{5}$ Nm^{-1} $k^{(4)}_{B_{2,1}}=5\times10^{5}$ Nm^{-1}
Nodal spring	$k^{(N_3)}=5\times10^{5}$ Nm^{-1}			
Mesh 1	2	4	3	3
Mesh 2	18	36	18	18
Mesh 3	30	60	30	30

For free and forced vibrations, the exact proposed method is implemented in Mathematica [52] considering 4 members including mass-spring subsystems/joints/springs and 3 member-to-member nodes with nonzero degrees of freedom (N_1, N_2, N_3 in Figure 3), i.e. the size of the corresponding global dynamic stiffness matrix given by Eq.(19) is 9×9. For comparison, a FE model is implemented in ADINA [53] using standard two-node Euler-Bernoulli elements. Three meshes are considered with increasing refinement, as detailed in Table 1. A conventional lumped mass matrix is assumed for all meshes. Specifically for free vibrations, a comparison is made also with the exact method proposed by Dias and Alves in ref. [32]. The method is implemented considering nodes N_1, N_2, N_3 in Figure 3 along with the following nodes: two nodes for the mass-spring subsystem in member 1 (= one at the application point on the member + one for the mass); three nodes for the mass-spring subsystem in member 2 (= one at the application point on the member + one for mass

$M_{B_{2,1}}^{(2)}$ + one for mass $M_{B_{2,2}}^{(2)}$); one node at the application point of each spring within member 4; one node at $x=0$ and one node at $x=L^{(2)}$ within member 2. The nodes are connected by continuous members, according to the geometry in Figure 3; the nodes at $x=0$ and $x=L^{(2)}$ within member 2 are connected to node N_2 and node N_3 respectively by rotational spring elements, while the springs of the mass-spring subsystems are modelled by translational spring elements. Finally, as explained in ref. [32] (see Eq.(24) therein), the model includes concentrated inertia forces on every mass of the mass-spring subsystems (in axial and transverse directions relative to the members, based on mass data in Table 1), as well as the elastic reaction forces of the spring at node N_3 and the springs within member 4. Natural frequencies from the resulting eigenvalue matrix are effectively computed using the numerical algorithm in ref. [32].

Table 2 shows the natural frequencies of the first 15 modes, as computed by the proposed method using the dynamic stiffness matrix given by Eq.(19), the FE method with various meshes and the method in ref. [32]. As expected, the accuracy of the FE method generally increases with mesh refinement. On the other hand, the exact proposed method and the exact method in ref. [32] provide almost coincident results, with differences only at the sixth or seventh digit; this is acceptable considering that the natural frequencies are obtained from different eigenvalue problems.

Table 2. Plane structure in Figure 3: Natural frequencies (Hz) of first 15 modes computed by proposed method, FE method for various meshes and method in ref. [32].

Mode	FE mesh 1	FE mesh 2	FE mesh 3	Exact method in ref. [32]	Exact proposed method
1	3.006087	3.006119	3.006119	3.006118	3.006118
2	4.597047	4.599482	4.599514	4.599524	4.599524
3	4.851106	4.851552	4.851552	4.851554	4.851553
4	8.014343	8.014550	8.014565	8.014561	8.014560
5	8.950269	8.971007	8.971278	8.971428	8.971427
6	15.12671	15.22198	15.22260	15.22298	15.22299
7	22.47968	24.36933	24.38604	24.39536	24.39538
8	91.81139	94.17055	94.17548	94.17876	94.17877
9	112.1127	127.4981	127.5749	127.6175	127.6177
10	134.7199	145.8798	145.9806	146.0376	146.0378
11	156.6352	166.3074	166.3424	166.3622	166.3625
12	161.3099	171.9001	172.0545	172.1444	172.1446
13	221.3670	225.6499	225.6929	225.7158	225.7161
14	299.8081	301.2214	301.2835	301.3171	301.3173
15	338.8361	337.2334	337.4069	337.5030	337.5033

Figure 4 shows the eigenfunctions for deflection, shear force and bending moment of the first mode in Table 2 along the continuous members, as computed by the proposed method using Eqs.(9)-(10) for every member. The eigenfunctions inherently satisfy all required conditions at the application points of mass-spring subsystems, joints and springs. Jump discontinuities occur in the shear force at the application points of mass-spring subsystems and springs, mirrored by slope discontinuities in the bending moment. Rotation discontinuities occur at the joints, see node 2 (nodal rotation in members 1-3 is equal but different from that in member 2) and node 3 (nodal rotations are different in members 2 and 4). Based on Eqs.(9)-(10) the eigenfunctions can be computed for all response variables along the continuous members, while displacements of the mass-spring subsystems can be obtained from the deflection/axial-displacement of the application point, using the free-vibration equilibrium equations of the masses [17,18].

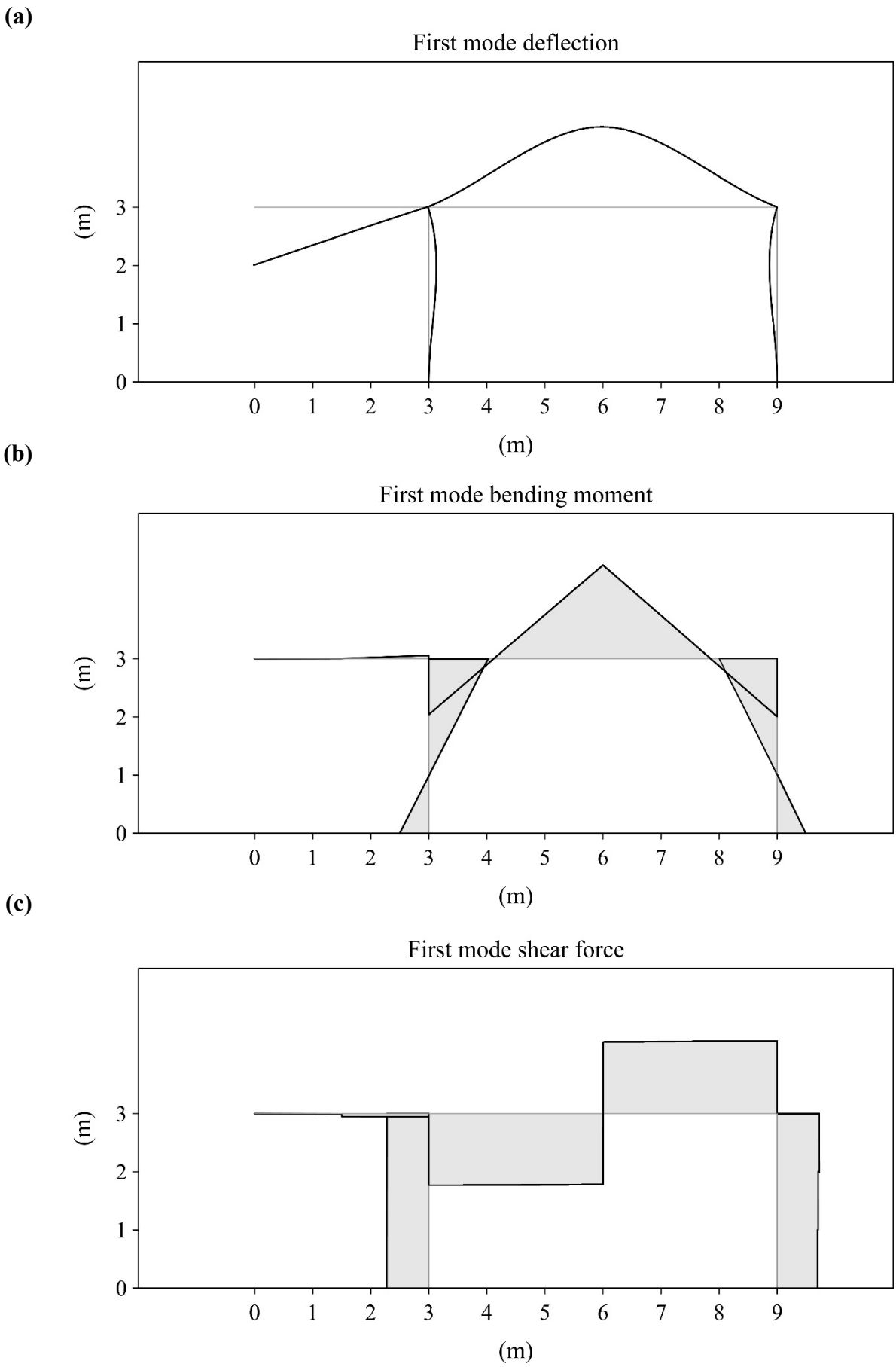

Figure 4. First mode deflection (a), bending moment (b) and shear force (c) for plane structure in Figure 3, as computed by proposed method.

Once natural frequencies and modes are calculated, proposed method and FE method are applied to investigate the dynamic response under a unit uniform load applied over member 3. Specifically, the response is computed using the 15 modes in Table 2, assuming the following modal damping ratios: $\zeta_i = 1\%$ for *i*=1,2,...5 and $\zeta_i = 2\%$ for *i*=6,2,...15.

Figure 5 shows the frequency response amplitude for the transverse displacement of mass $M_{B_{2,2}}^{(2)}$ in member 2, when the forcing frequency of the unit uniform load over member 3 varies over the frequency range 0-30 Hz. In particular, Figure 5a shows the proposed solution in Eq.(82) including the single modal frequency responses as well as the total frequency response built with 15 modes. Then, Figure 5b shows the total frequency response built with 15 modes, as computed by the proposed method using Eq.(82) and the FE method with Meshes 1-2-3. It is apparent that the accuracy of the FE models increases with mesh refinement. However, significant discrepancies are encountered for Mesh 1 above 20 Hz, while proposed method and FE method agree very well for Mesh 2 and Mesh 3, with an excellent matching for Mesh 3. For a further insight, Figure 6 shows the frequency response amplitude for the transverse displacement of mass $M_{B_{2,2}}^{(2)}$ in member 2, over the frequency range 0-400 Hz. Peaks are grouped over certain frequency ranges, as is typically the case in continuous structures coupled with mass-spring subsystems, and contribution of lower modes is significant also at high frequency range. It is evident that Mesh 1 does not provide accurate results while, in contrast, a very good agreement with the proposed solution given by Eq.(82) is obtained for Mesh 2 and Mesh 3; again, an excellent matching is seen for Mesh 3.

Additional results in terms of frequency response are reported in Figure 7 through Figure 10, for rotation of the right end section of member 2 and bending moment at the base section of member 3. For both, discrepancies between the proposed solution given by Eq.(82) and the FE solution obtained with Mesh 1 are significant over the whole frequency range, while a very satisfactory agreement is found between the proposed solution given by Eq.(82) and FE solutions for Mesh 2 and Mesh 3, with an excellent matching for Mesh 3.

(a)

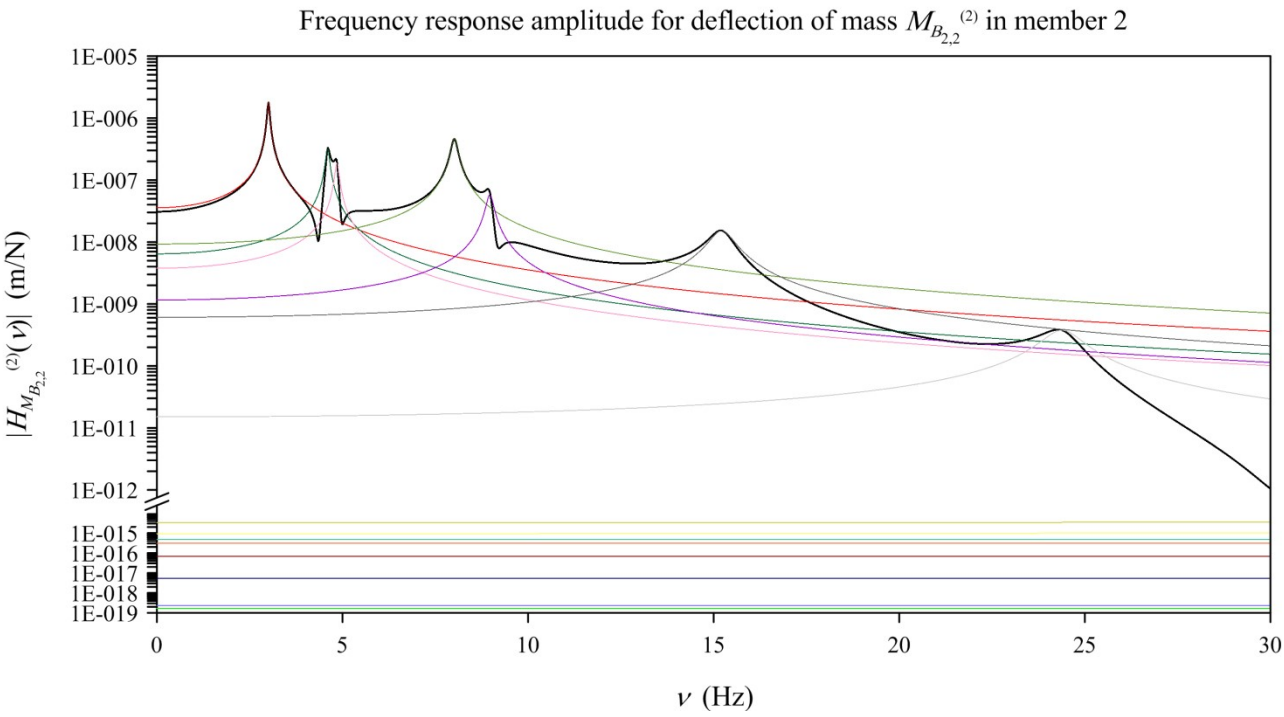

(b)

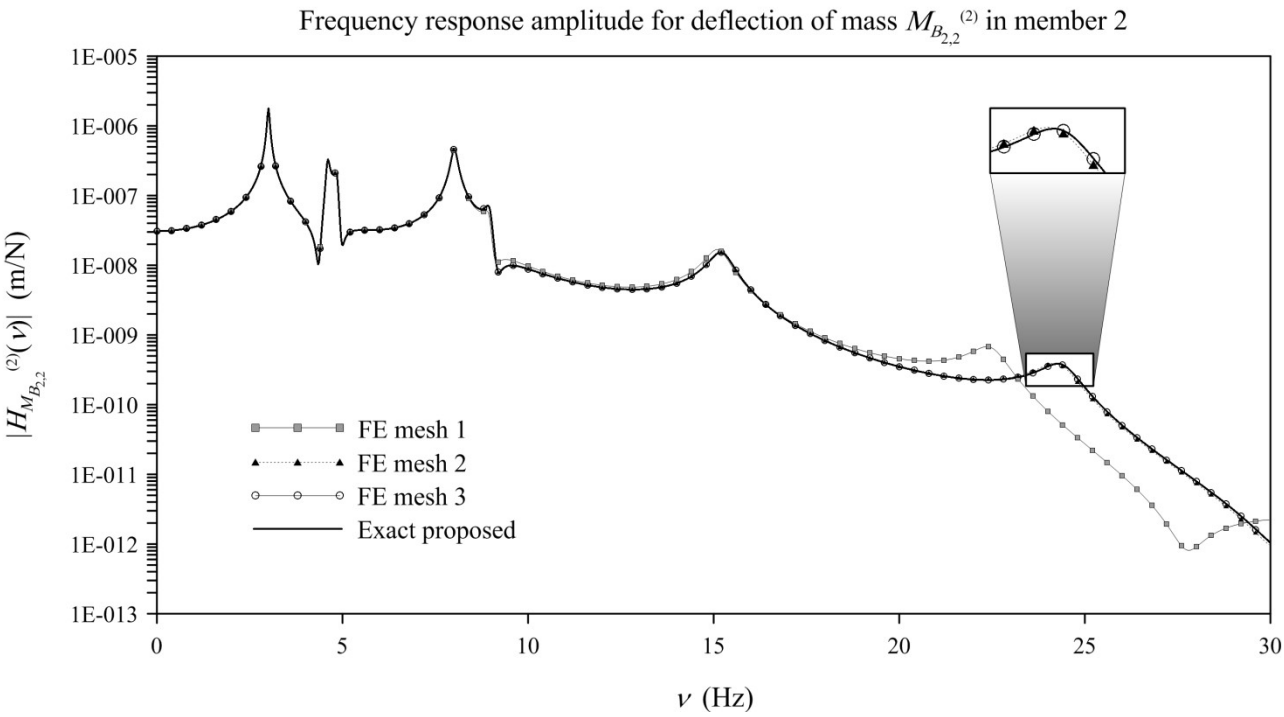

Figure 5. Frequency response amplitude for deflection of mass $M_{B_{2,2}}^{(2)}$ in member 2 over 0-30 Hz, computed with 15 modes in Table 2: (a) total modal response (black line) and single modal responses (colour lines) by proposed method; (b) total modal response by proposed method and FE method for various meshes.

(a)

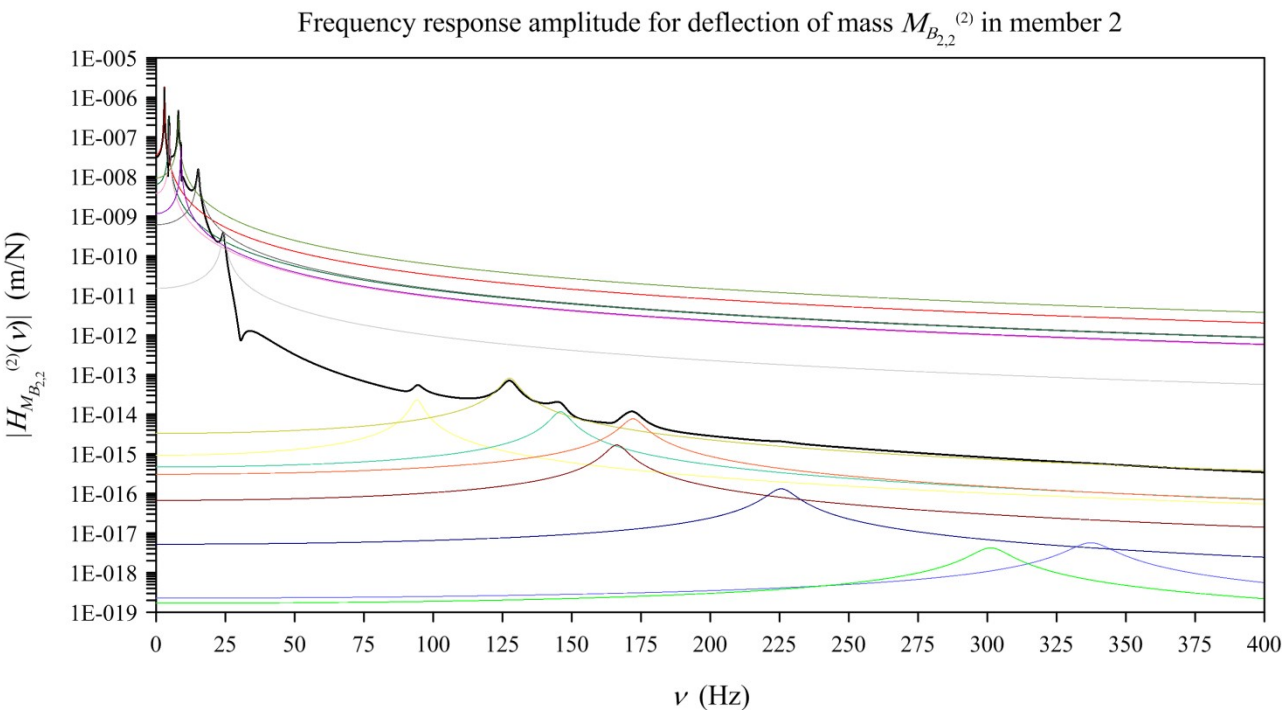

(b)

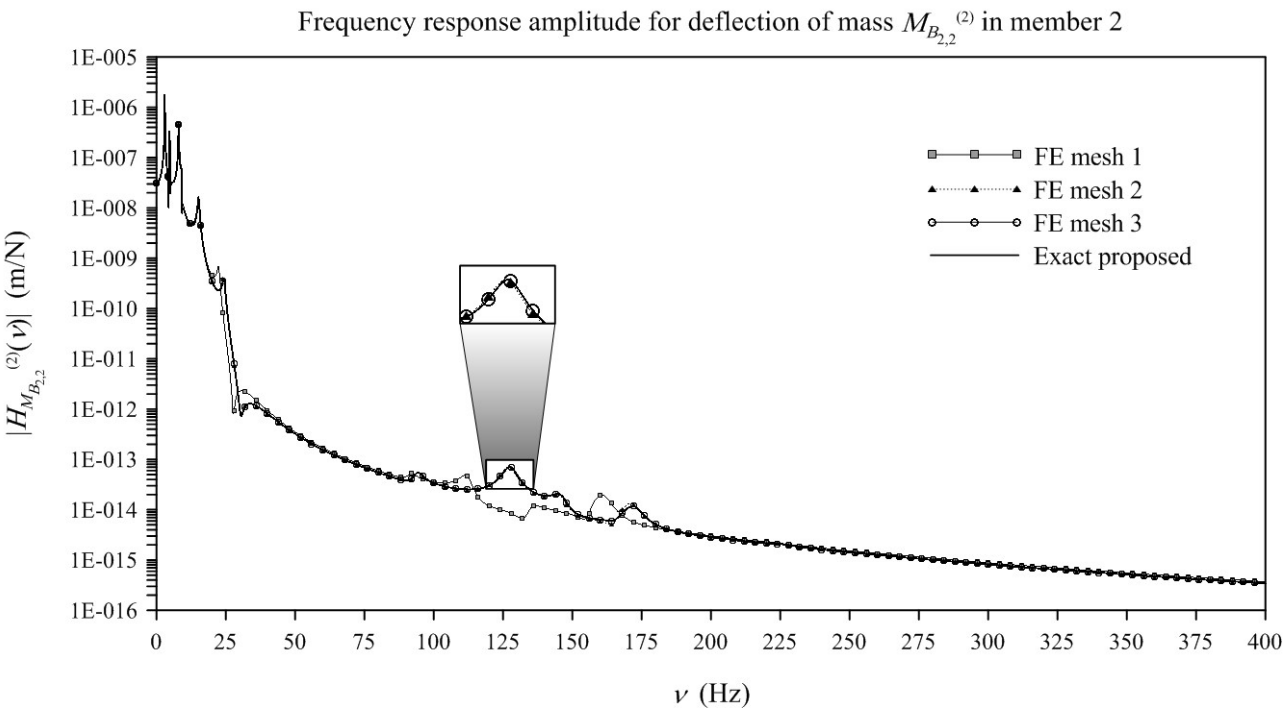

Figure 6. Frequency response amplitude for deflection of mass $M_{B_{2,2}}^{(2)}$ in member 2 over 0-400 Hz, computed with 15 modes in Table 2: (a) total modal response (black line) and single modal responses (colour lines) by proposed method; (b) total modal response by proposed method and FE method for various meshes.

(a)

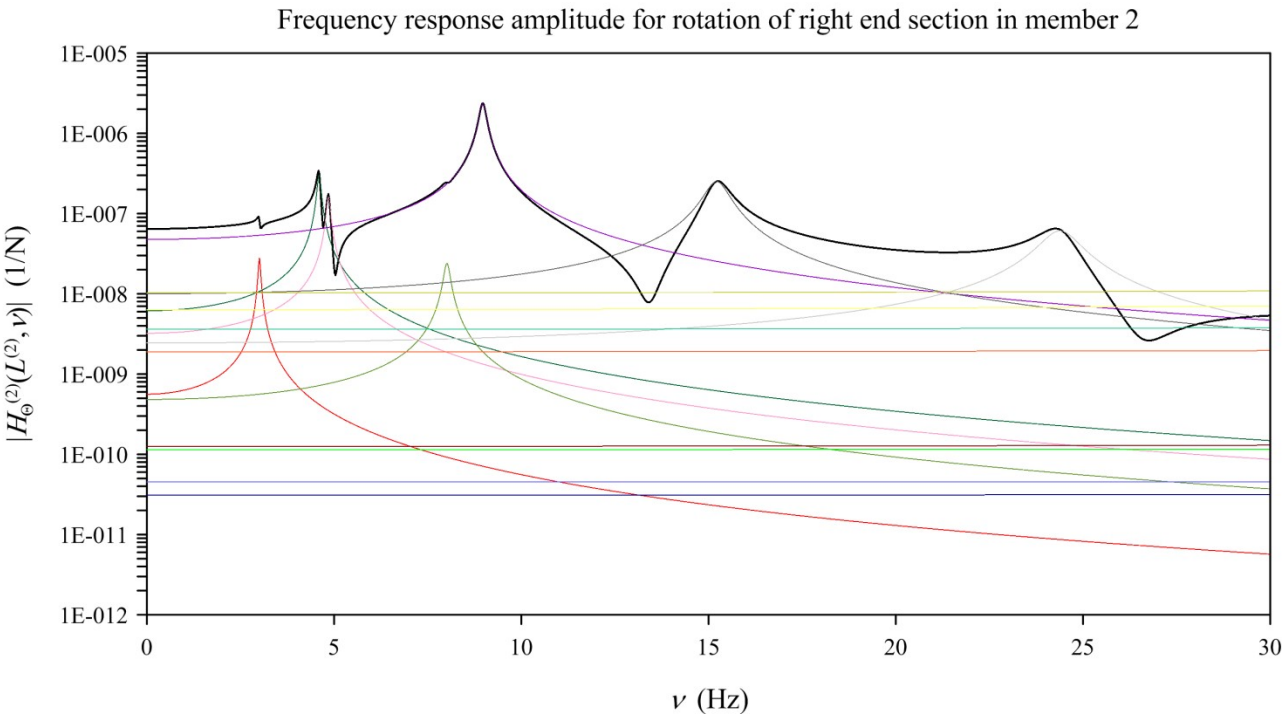

(b)

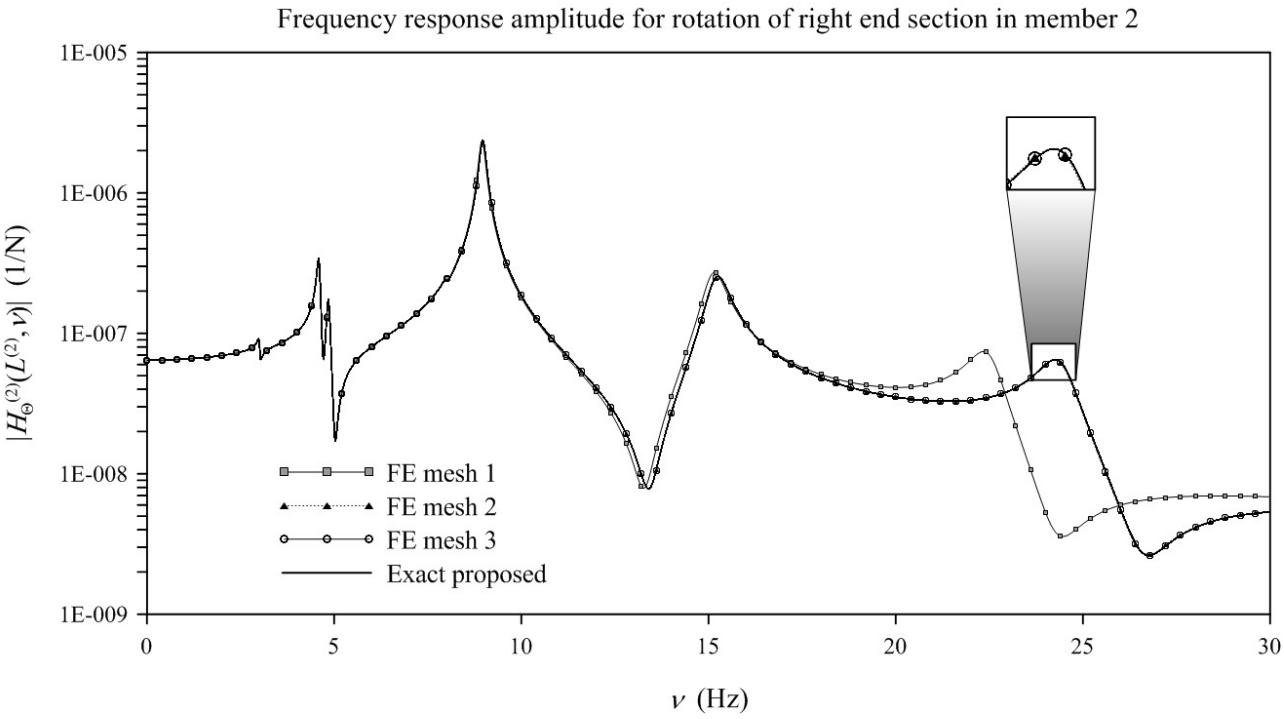

Figure 7. Frequency response amplitude for rotation of right end section in member 2 over 0-30 Hz, computed with 15 modes in Table 2: (a) total modal response (black line) and single modal responses (colour lines) by proposed method; (b) total modal response by proposed method and FE method for various meshes.

(a)

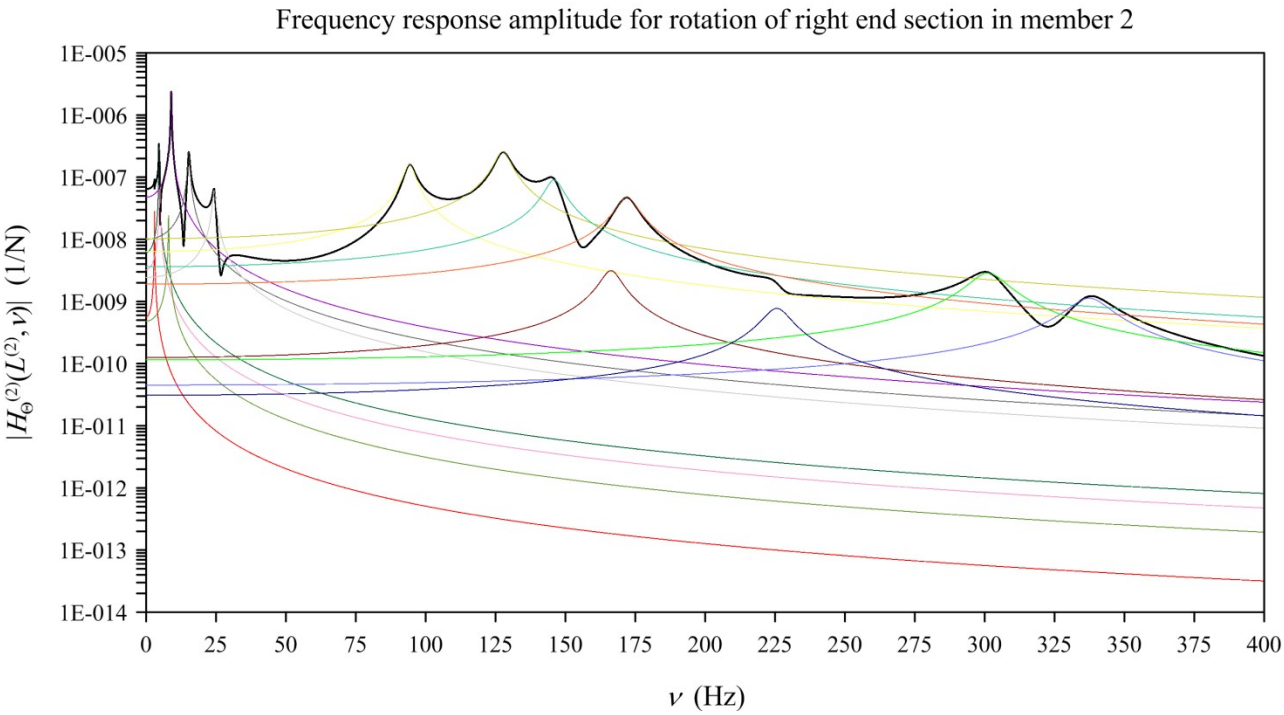

(b)

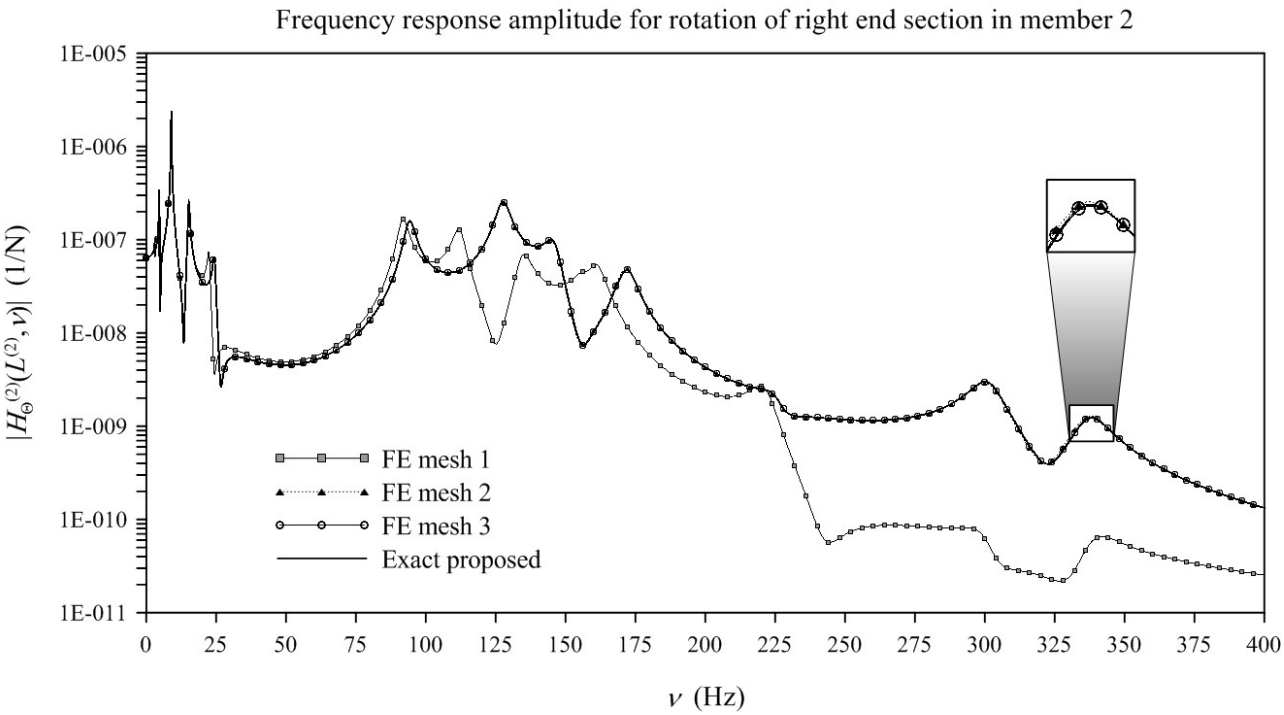

Figure 8. Frequency response amplitude for rotation of right end section in member 2 over 0-400 Hz, computed with 15 modes in Table 2: (a) total modal response (black line) and single modal responses (colour lines) by proposed method; (b) total modal response by proposed method and FE method for various meshes.

(a)

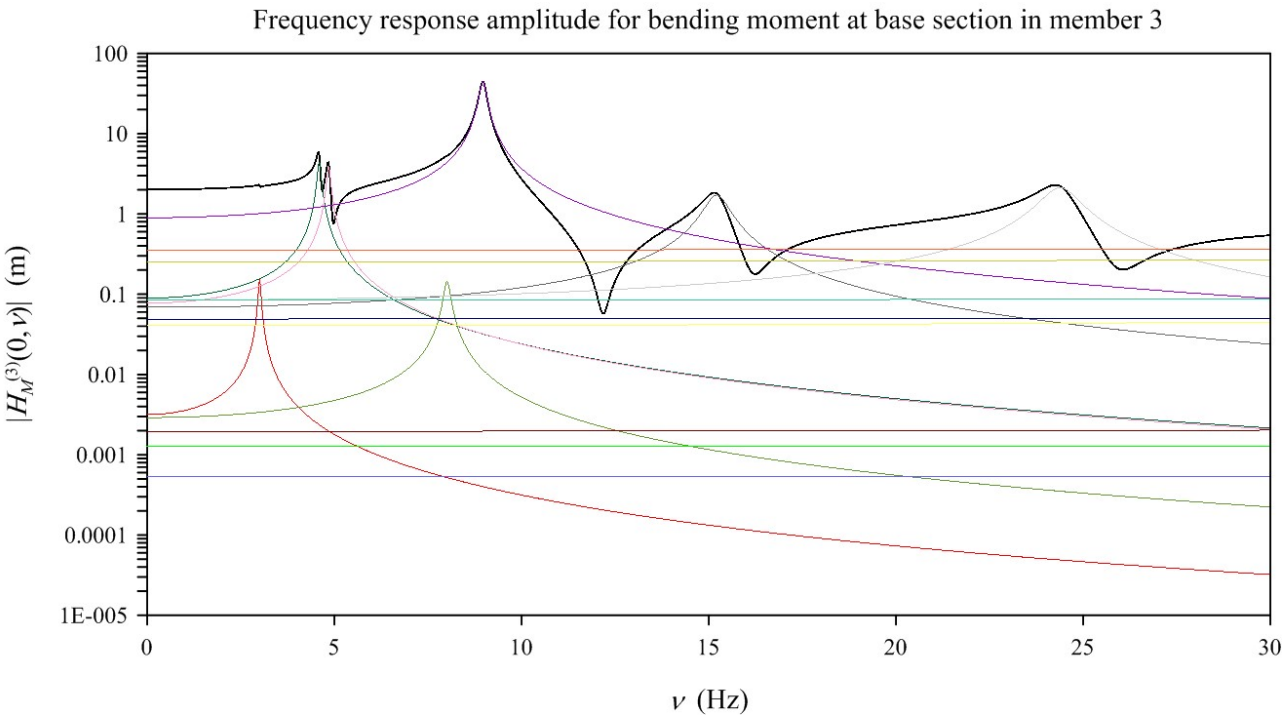

(b)

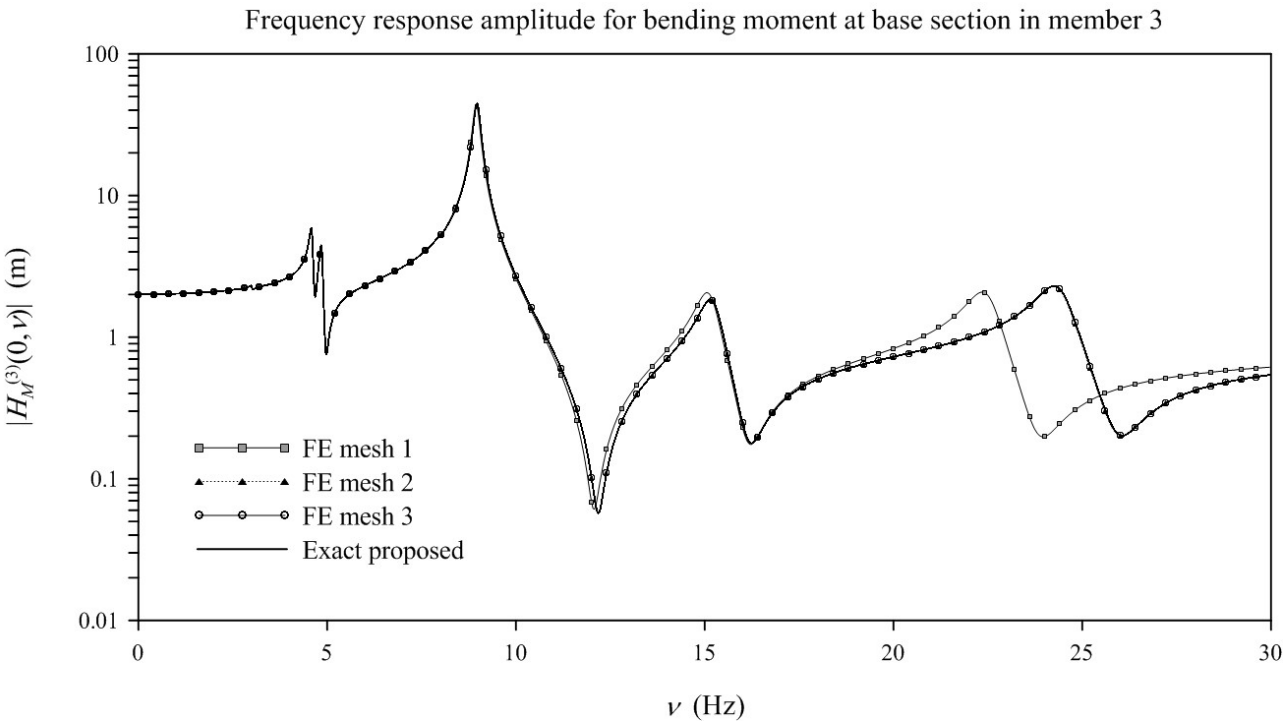

Figure 9. Frequency response amplitude for bending moment at base section in member 3 over 0-30 Hz, computed with 15 modes in Table 2: (a) total modal response (black line) and single modal responses (colour lines) by proposed method; (b) total modal response by proposed method and FE method for various meshes.

(a)

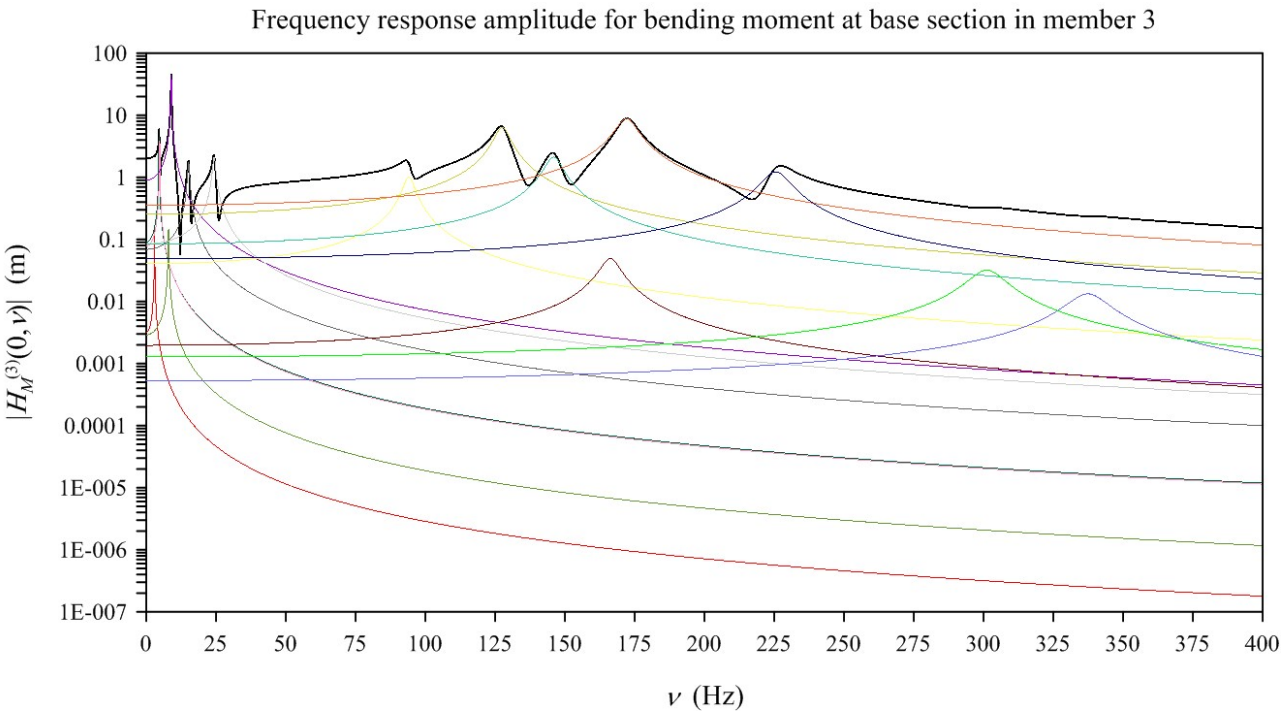

(b)

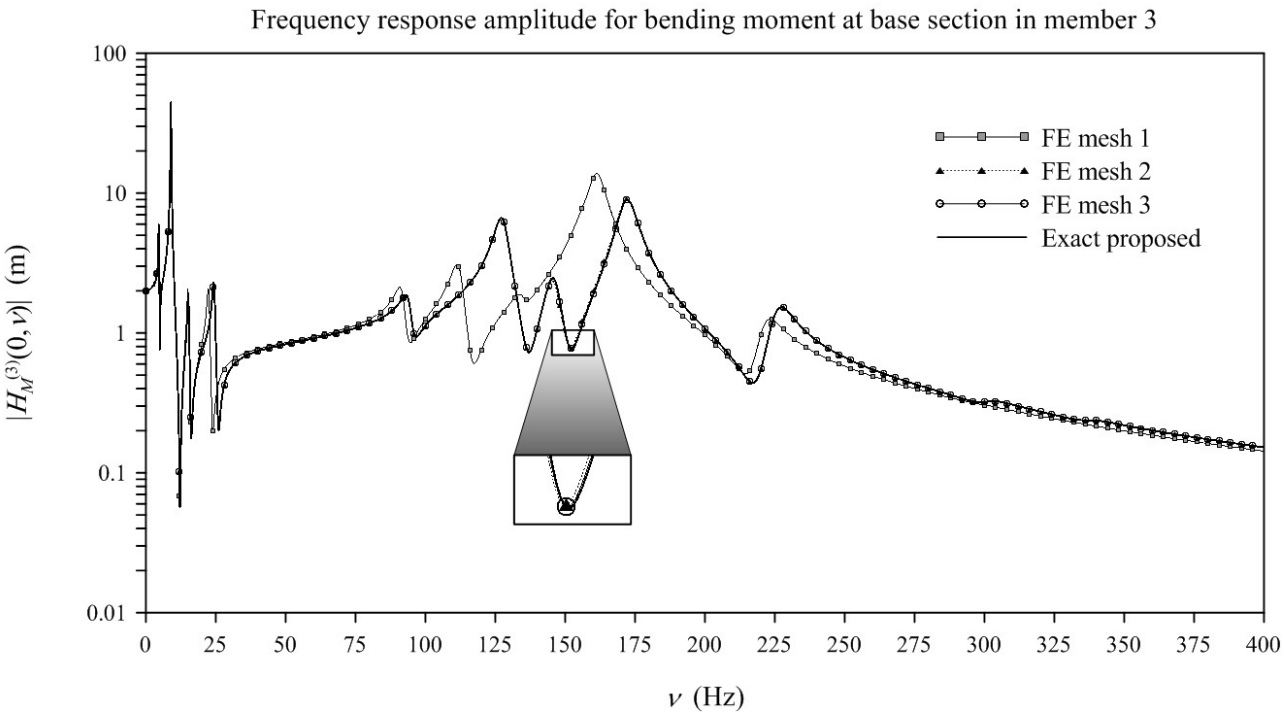

Figure 10. Frequency response amplitude for bending moment at base section in member 3 over 0-400 Hz, computed with 15 modes in Table 2: (a) total modal response (black line) and single modal responses (colour lines) by proposed method; (b) total modal response by proposed method and FE method for various meshes.

Next, Figure 11 shows the frequency response amplitude for the shear force along member 1, when the forcing frequency of the unit uniform load over member 3 is 10 Hz. In particular, Figure 11a shows that the proposed solution given by Eq.(82) varies as the number of modes increases, and that no significant differences are encountered between when 13 or 15 modes are considered. Then, Figure 11b compares the proposed solution given by Eq.(82) built with 15 modes to the corresponding one obtained by the FE method with Meshes 1-2-3. The FE method provides a stepwise approximation of the shear force over every finite element. While results obtained with Mesh 1 are rather inaccurate, a good agreement is encountered between proposed solution given by Eq.(82) and FE ones for Mesh 2 and Mesh 3, especially for Mesh 3. Similar observations can be made in Figure 12, which shows the axial force along member 1 when the forcing frequency of the unit uniform load over member 3 is equal to 5 Hz. In this case, the agreement between the proposed solution given by Eq.(82) and FE solutions for Mesh 2 and Mesh 3 is even better than that in Figure 11.

Finally, Figure 13 shows the time histories of some response variables, when the unit uniform load over member 3 is a sine load with various forcing frequencies. Specifically, transverse displacement of mass $M_{B_{2,1}}^{(2)}$ in member 2 and bending moment at base section in member 3 are computed by the proposed method using Eq.(80), as well as the FE method with Meshes 1-2-3. Results are in agreement with those in Figure 5 through Figure 10, that is large discrepancies may be found between the proposed solution given by Eq.(80) and FE one for Mesh 1 while, instead, a very satisfactory agreement is found when Mesh 2 and Mesh 3 are used; again, an excellent matching is obtained for Mesh 3, as for the frequency response in Figures 5-10.

Based on the results in Figures 5 through 13, it may be stated that the exact proposed solutions represent a benchmark for FE solutions with various meshes, in both time and frequency domain.

(a)

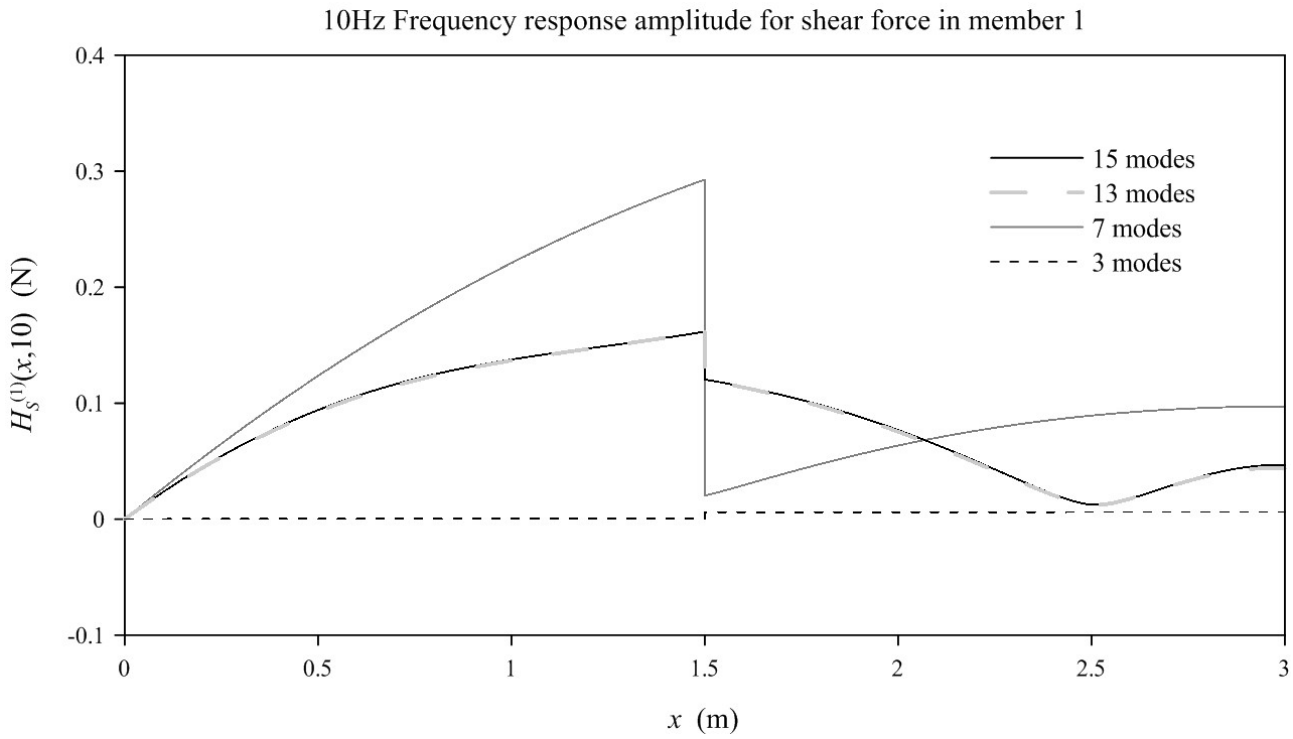

(b)

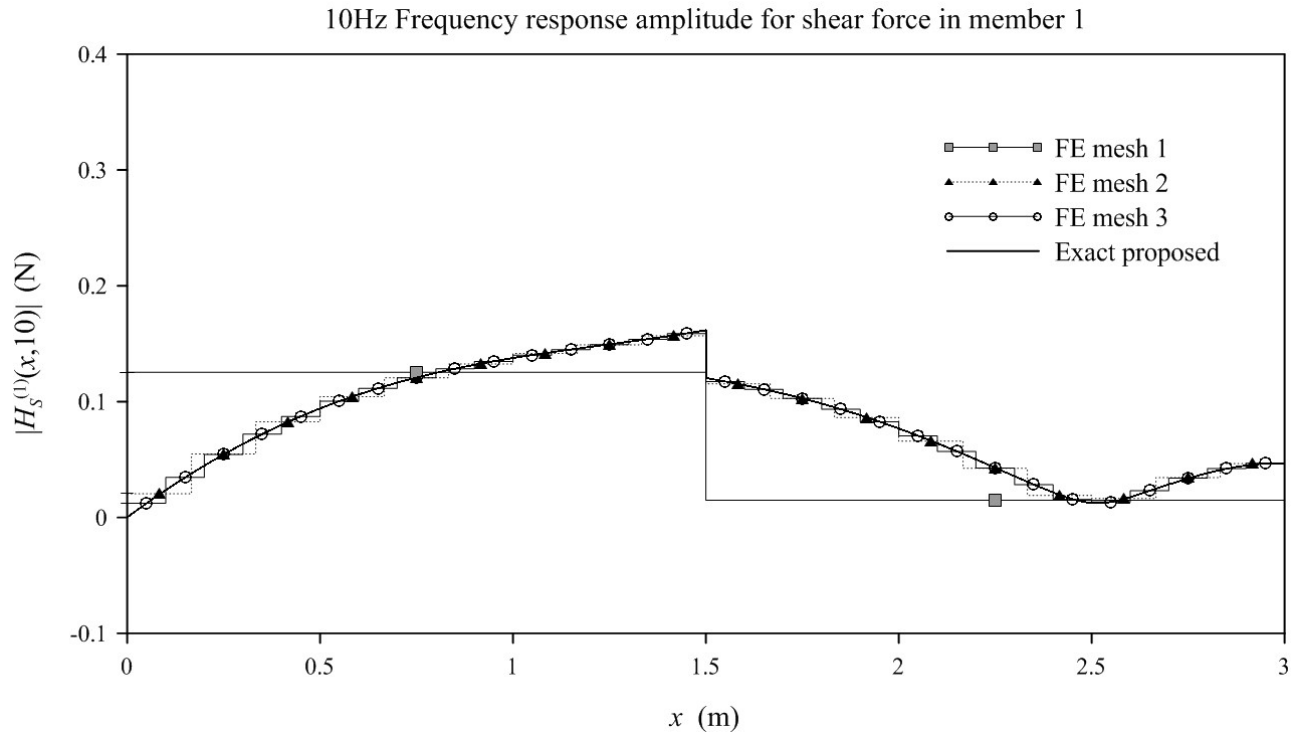

Figure 11. 10Hz Frequency response amplitude for shear force in member 1: (a) proposed method with different number of modes in Table 2; (b) proposed method and FE method with 15 modes in Table 2.

(a)

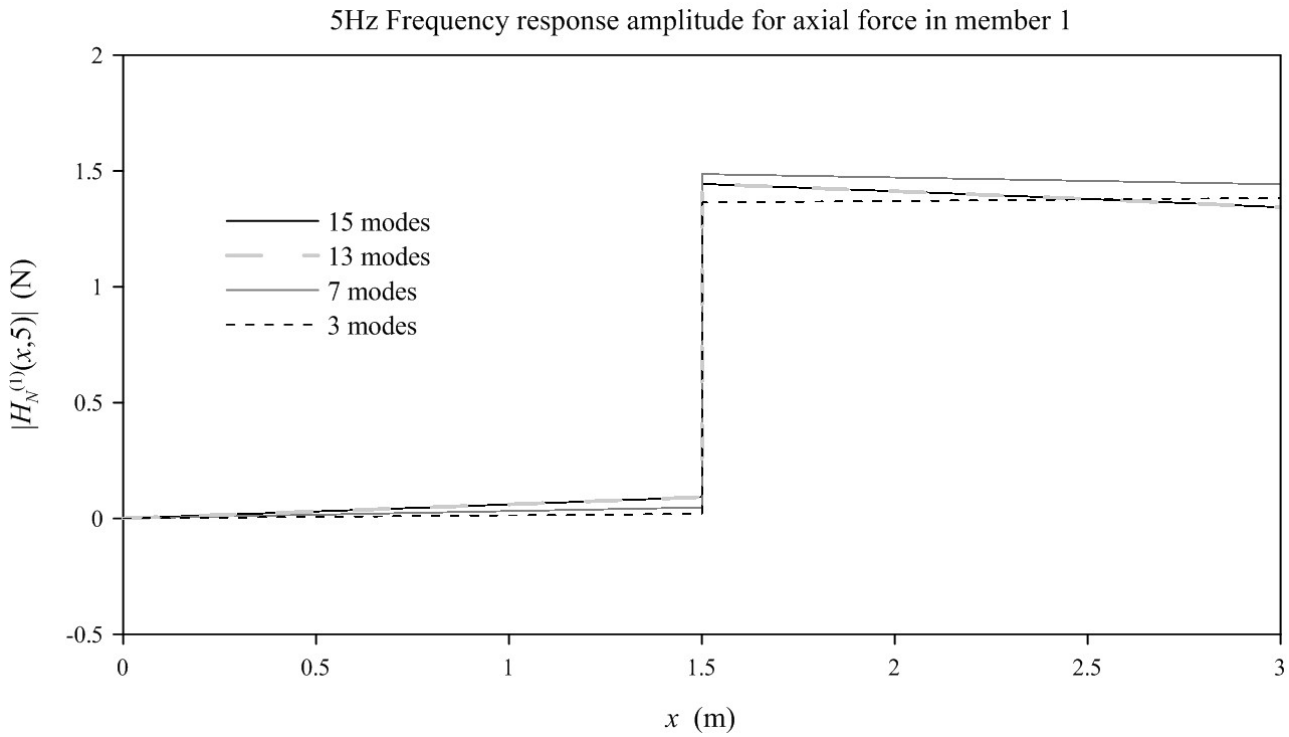

(b)

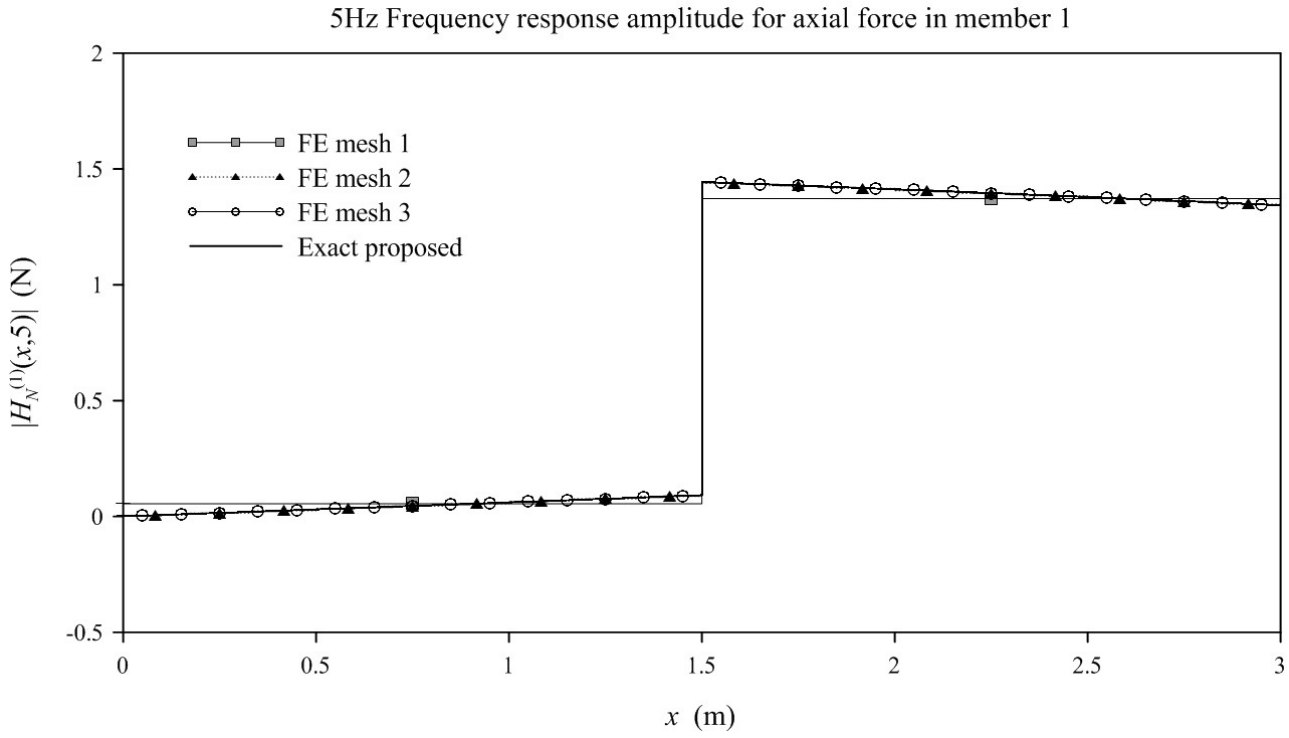

Figure 12. 5Hz Frequency response amplitude for axial force in member 1: (a) proposed method with different number of modes in Table 2; (b) proposed method and FE method with 15 modes in Table 2.

(a)

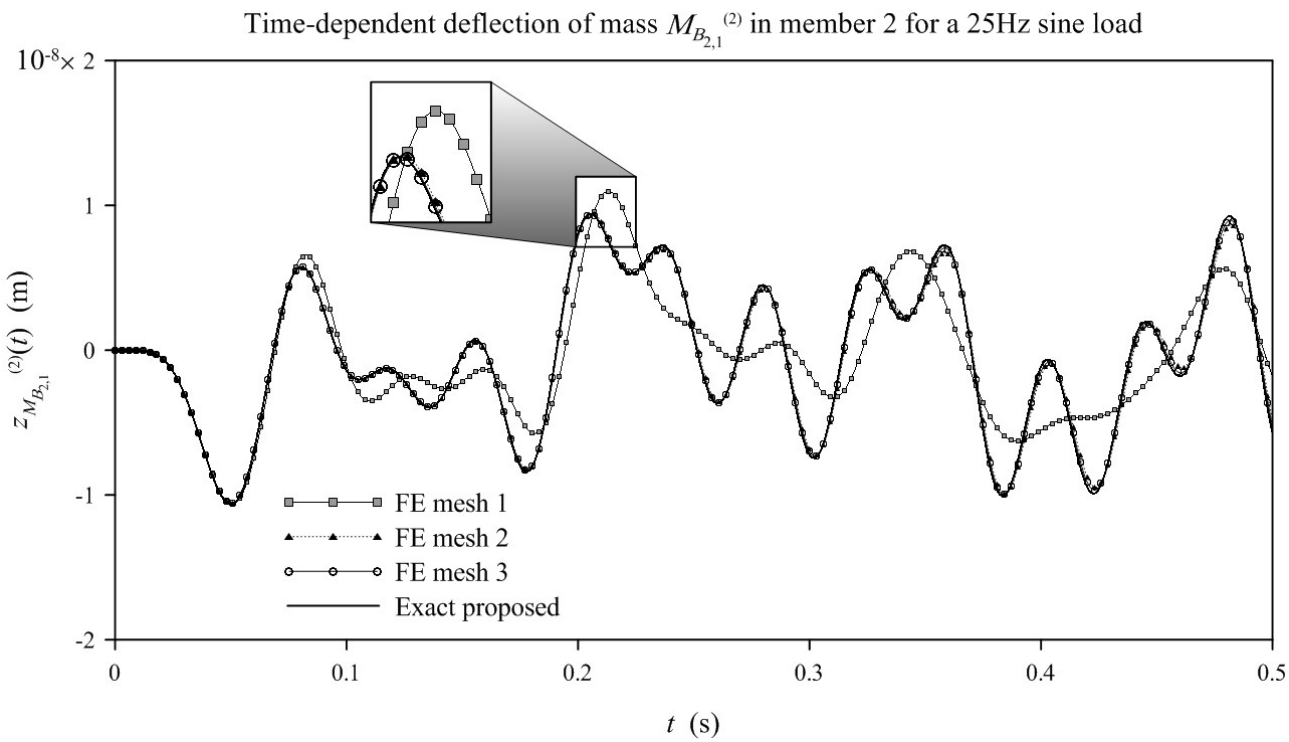

(b)

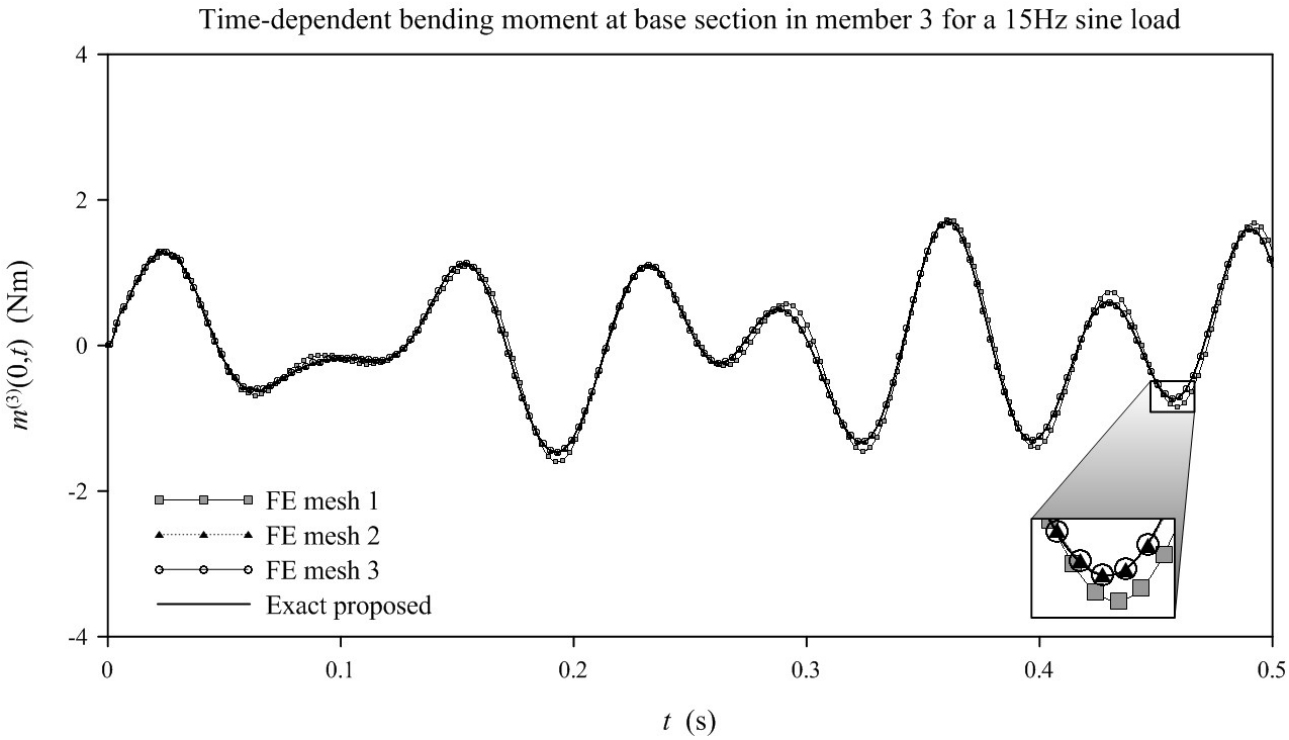

Figure 13. Time-dependent response computed with 15 modes in Table 2 by proposed method and FE method with various meshes: (a) deflection of mass $M_{B_{2,1}}^{(2)}$ in member 2 for a 25Hz sine load; (b) bending moment at base section in member 3 for a 15Hz sine load.

7. CONCLUSIONS

An exact modal analysis approach has been presented for vibration analysis of plane continuous structures, which are coupled with mass-spring subsystems and include elastic rotational joints. Typical mass-spring subsystems have been considered, starting from the general case of a three-mass-three-spring subsystem acting in transverse and axial directions relative to every continuous member.

The main results of the proposed approach are: (a) every member with arbitrary number of mass-spring subsystems and joints can be treated as a two-node element, with 6×6 exact dynamic stiffness matrix obtained in closed form; (b) exact natural frequencies of the undamped modes can be obtained from a global dynamic stiffness matrix with size depending only on the number of nonzero nodal degrees of freedom of member-to-member nodes; (c) motion equations can be decoupled based on pertinent orthogonality conditions for the modes, obtaining modal impulse and modal frequency response functions in closed analytical form, to be used for vibration analysis under arbitrary loads on the assumption of proportional damping. As a result, simple analytical forms have been derived to compute any response variable of the system, in time and frequency domain. Solutions are exact and serve as benchmark for classical FE solutions, as shown by numerical results.

As for generalizations of the method to alternative subsystems attached to the continuous members, it has been shown that the method applies provided that a frequency-dependent stiffness given as Eq.(5) is defined and the corresponding limit in Eq.(65) exists for the subsystem. These conditions are generally fulfilled by discrete multi-mass-multi-spring subsystems, whose frequency-dependent stiffness involves polynomial functions of the frequency.

8. APPENDIX A

For every mode, matrices $\tilde{\mathbf{W}}_B^{(i)}(x)$ and $\tilde{\mathbf{W}}_A^{(i)}(x)$ in Eqs.(9)-(10) are given as

$$\tilde{\mathbf{W}}_B^{(i)}(x) = \tilde{\mathbf{\Omega}}_B^{(i)}(x) + \sum_{j=1}^{N^{(i)}} \tilde{\mathbf{J}}_B^{(i)}\left(x, x_j^{(i)}\right) \tilde{\mathbf{\Phi}}_{\mathbf{\Omega}_B}^{(i)}\left(x_j^{(i)}\right) + \sum_{2 \le q \le j} \tilde{\mathbf{J}}_B^{(i)}\left(x, x_j^{(i)}\right) \sum_{(j,m,n,\ldots,r,s) \in \mathbb{N}_q^{(j)}} \tilde{\mathbf{\Phi}}_{\mathbf{J}_B}^{(i)}\left(x_j^{(i)}, x_m^{(i)}\right) \tilde{\mathbf{\Phi}}_{\mathbf{J}_B}^{(i)}\left(x_m^{(i)}, x_n^{(i)}\right) \cdots \tilde{\mathbf{\Phi}}_{\mathbf{J}_B}^{(i)}\left(x_r^{(i)}, x_s^{(i)}\right) \tilde{\mathbf{\Phi}}_{\mathbf{\Omega}_B}^{(i)}\left(x_s^{(i)}\right) \tag{A.1}$$

$$\tilde{\mathbf{W}}_A^{(i)}(x)=\tilde{\mathbf{\Omega}}_A^{(i)}(x)+\sum_{j=1}^{N^{(i)}}\tilde{\mathbf{J}}_A^{(i)}\left(x,x_j^{(i)}\right)\tilde{\mathbf{\Phi}}_{\mathbf{\Omega}_A}^{(i)}\left(x_j^{(i)}\right)+$$
$$\sum_{2\le q\le j}\tilde{\mathbf{J}}_A^{(i)}\left(x,x_j^{(i)}\right)\sum_{(j,m,n,\ldots,r,s)\in\mathbb{N}_q^{(j)}}\tilde{\Phi}_{\mathbf{J}_A}^{(i)}\left(x_j^{(i)},x_m^{(i)}\right)\tilde{\Phi}_{\mathbf{J}_A}^{(i)}\left(x_m^{(i)},x_n^{(i)}\right)\cdots\tilde{\Phi}_{\mathbf{J}_A}^{(i)}\left(x_r^{(i)},x_s^{(i)}\right)\tilde{\mathbf{\Phi}}_{\mathbf{\Omega}_A}^{(i)}\left(x_s^{(i)}\right) \tag{A.2}$$

where $\mathbb{N}_q^{(j)}=\{\ (\underbrace{j,m,n,\ldots r,s}_{q}):j>m>n>\ldots>r>s;\ m,n,\ldots r,s=1,2,\ldots,(j-1)\ \}$ is the set including all possible q-ples of indexes $(\underbrace{j,m,n,\ldots r,s}_{q})$ such that $j>m>n>\ldots>r>s$, being $2\le q\le j$.

In Eqs.(A.1)-(A.2), $\tilde{\mathbf{J}}_B^{(i)}\left(x,x_j^{(i)}\right)$ and $\tilde{\mathbf{J}}_A^{(i)}\left(x,x_j^{(i)}\right)$ are the 4×2 matrix and 2×1 vector

$$\tilde{\mathbf{J}}_B^{(i)}\left(x,x_j^{(i)}\right)=\begin{bmatrix}\tilde{J}_{V,P}^{(i)} & \tilde{J}_{V,\Delta\Theta}^{(i)}\\ \tilde{J}_{\Theta,P}^{(i)} & \tilde{J}_{\Theta,\Delta\Theta}^{(r)}\\ \tilde{J}_{M,P}^{(i)} & \tilde{J}_{M,\Delta\Theta}^{(r)}\\ \tilde{J}_{S,P}^{(i)} & \tilde{J}_{S,\Delta\Theta}^{(r)}\end{bmatrix}\qquad \tilde{\mathbf{J}}_A^{(i)}\left(x,x_j^{(i)}\right)=\begin{bmatrix}\tilde{J}_{U,P}^{(i)}\\ \tilde{J}_{N,P}^{(i)}\end{bmatrix} \tag{A.3a,b}$$

while symbols $\tilde{\mathbf{\Phi}}_{\mathbf{J}_B}^{(i)}\left(x_j^{(i)},x_k^{(i)}\right)$ and $\tilde{\Phi}_{\mathbf{J}_A}^{(i)}\left(x_j^{(i)},x_k^{(i)}\right)$ denote the following 2×2 matrix and scalar function:

$$\tilde{\mathbf{\Phi}}_{\mathbf{J}_B}^{(i)}\left(x_j^{(i)},x_k^{(i)}\right)=\begin{bmatrix}-\kappa_{B_j}^{(i)}(\omega)\left(\tilde{\mathbf{J}}_B^{(i)}\left(x_j^{(i)},x_k^{(i)}\right)\right)_1\\ -\left(k_{\Delta\Theta_j}^{(i)}\right)^{-1}\left(\tilde{\mathbf{J}}_B^{(i)}\left(x_j^{(i)},x_k^{(i)}\right)\right)_3\end{bmatrix}\quad \tilde{\Phi}_{\mathbf{J}_A}^{(i)}\left(x_j^{(i)},x_k^{(i)}\right)=-\kappa_{A_j}^{(i)}(\omega)\left(\tilde{\mathbf{J}}_A^{(i)}\left(x_j^{(i)},x_k^{(i)}\right)\right)_1 \tag{A.4a,b}$$

where notation $(\cdot)_l$ indicates the lth row of the matrix within parenthesis. All terms of $\tilde{\mathbf{J}}_B^{(i)}\left(x,x_j^{(i)}\right)$ can readily be derived from the beam equations

$$\frac{\bar{\mathrm{d}}\tilde{S}^{(i)}(x)}{\mathrm{d}x}+\sum_{j=1}^{N}\tilde{R}_{B_j}^{(i)}\delta\left(x-x_j^{(i)}\right)+\rho^{(i)}\omega^2\tilde{V}^{(i)}(x)=0\qquad \frac{\bar{\mathrm{d}}\tilde{M}^{(i)}(x)}{\mathrm{d}x}=\tilde{S}^{(i)}(x) \tag{A.5a,b}$$

$$\frac{\overline{\mathrm{d}}\tilde{\Theta}^{(i)}(x)}{\mathrm{d}x} = -\frac{\tilde{M}^{(i)}(x)}{EI^{(i)}} + \sum_{j=1}^{N^{(i)}} \Delta\tilde{\Theta}_j^{(i)} \delta\left(x - x_j^{(i)}\right) \qquad \frac{\overline{\mathrm{d}}\tilde{V}^{(i)}(x)}{\mathrm{d}x} = \tilde{\Theta}^{(i)}(x) \tag{A.6a,b}$$

starting from the following particular integrals for deflection associated with a unit force and a unit relative rotation at arbitrary $x = x_0^{(i)}$:

$$\tilde{J}_{V,P}^{(i)}\left(x, x_0^{(i)}\right) = \alpha\left(\sinh\left(\beta\left(x - x_0^{(i)}\right)\right) - \sin\left(\beta\left(x - x_0^{(i)}\right)\right)\right) H\left(x - x_0^{(i)}\right) \tag{A.7}$$

$$\tilde{J}_{V,\Delta\Theta}^{(i)}\left(x, x_0^{(i)}\right) = EI^{(i)} \alpha\beta^2 \left(\sinh\left(\beta\left(x - x_0^{(i)}\right)\right) + \sin\left(\beta\left(x - x_0^{(i)}\right)\right)\right) H\left(x - x_0^{(i)}\right) \tag{A.8}$$

where $\alpha = \alpha^{(i)} = 2^{-1}\left(EI^{(i)}\right)^{-1/4}\left(\rho^{(i)}\right)^{-3/4}\omega^{-3/2}$ and $\beta = \beta^{(i)} = \left(EI^{(i)}\right)^{-1/4}\left(\rho^{(i)}\right)^{1/4}\omega^{1/2}$. Likewise, terms of $\tilde{\mathbf{J}}_A^{(i)}\left(x, x_j^{(i)}\right)$ can be derived from the beam equations

$$\frac{\overline{\mathrm{d}}\tilde{N}^{(i)}(x)}{\mathrm{d}x} + \sum_{j=1}^{N^{(i)}} \tilde{R}_{A_j}^{(i)} \delta\left(x - x_j^{(i)}\right) + \rho^{(i)}\omega^2 \tilde{U}^{(i)}(x) = 0; \qquad \frac{\overline{\mathrm{d}}\tilde{U}^{(i)}(x)}{\mathrm{d}x} = \frac{\tilde{N}^{(i)}(x)}{EA^{(i)}} \tag{A.9a,b}$$

starting from the following particular integral for axial displacement, associated with a unit force at $x = x_0^{(i)}$:

$$\tilde{J}_{U,P}^{(i)}\left(x, x_0^{(i)}\right) = -\lambda \sin\left(\eta\left(x - x_0^{(i)}\right)\right) H\left(x - x_0^{(i)}\right) \tag{A.10}$$

being $\lambda = \lambda^{(i)} = \left(EA^{(i)}\right)^{-1/2}\left(\rho^{(i)}\right)^{-1/2}\omega^{-1}$ and $\eta = \eta^{(i)} = \left(EA^{(i)}\right)^{-1/2}\left(\rho^{(i)}\right)^{1/2}\omega$ frequency-dependent parameters.

Further, in Eqs.(A.1)-(A.2) $\tilde{\mathbf{\Omega}}_B^{(i)}(x)$ and $\tilde{\mathbf{\Omega}}_A^{(i)}(x)$ depend on the solutions to the homogeneous differential equations associated with Eq.(1) and Eq.(6), i.e.

$$\tilde{\mathbf{\Omega}}_B^{(i)}(x)=\begin{bmatrix} \mathrm{e}^{-\beta x} & \mathrm{e}^{\beta x} & \cos(\beta x) & \sin(\beta x) \\ -\beta \mathrm{e}^{-\beta x} & \beta \mathrm{e}^{\beta x} & -\beta \sin(\beta x) & \beta \cos(\beta x) \\ -EI\beta^2 \mathrm{e}^{-\beta x} & -EI\beta^2 \mathrm{e}^{\beta x} & EI\beta^2 \cos(\beta x) & EI\beta^2 \sin(\beta x) \\ EI\beta^3 \mathrm{e}^{-\beta x} & -EI\beta^3 \mathrm{e}^{\beta x} & -EI\beta^3 \sin(\beta x) & EI\beta^3 \cos(\beta x) \end{bmatrix} \tag{A.11}$$

$$\tilde{\mathbf{\Omega}}_A^{(i)}(x)=\begin{bmatrix} \cos(\eta x) & \sin(\eta x) \\ -EA^{(i)}\eta \sin(\eta x) & EA^{(i)}\eta \cos(\eta x) \end{bmatrix} \tag{A.12}$$

while $\tilde{\mathbf{\Phi}}_{\mathbf{\Omega}_B}^{(i)}\left(x_j^{(i)}\right)$ and $\tilde{\mathbf{\Phi}}_{\mathbf{\Omega}_A}^{(i)}\left(x_j^{(i)}\right)$ are the following 2×4 matrix and 1×2 row vector:

$$\tilde{\mathbf{\Phi}}_{\mathbf{\Omega}_B}^{(i)}\left(x_j^{(i)}\right)=\begin{bmatrix} -\kappa_{B_j}^{(i)}(\omega)\left(\tilde{\mathbf{\Omega}}_B^{(i)}\left(x_j^{(i)}\right)\right)_1 \\ -\left(k_{\Delta\Theta_j}^{(i)}\right)^{-1}\left(\tilde{\mathbf{\Omega}}_B^{(i)}\left(x_j^{(i)}\right)\right)_3 \end{bmatrix} \qquad \tilde{\mathbf{\Phi}}_{\mathbf{\Omega}_A}^{(i)}\left(x_j^{(i)}\right)=-\kappa_{A_j}^{(i)}(\omega)\left(\tilde{\mathbf{\Omega}}_A^{(i)}\left(x_j^{(i)}\right)\right)_1 \tag{A.13a,b}$$

Notice that terms in matrices $\tilde{\mathbf{\Omega}}_B^{(i)}\left(x_j^{(i)}\right)$ and $\tilde{\mathbf{\Omega}}_A^{(i)}\left(x_j^{(i)}\right)$ are derived from the well-known solutions to the homogeneous differential equations associated with Eq.(1) and Eq.(6) (among others, see ref. [45]), using Eqs.(A.5)-(A.6)-(A.9) without Dirac's deltas.

Changes whereas a single mass-spring subsystem or joint occurs at a given $x=x_j^{(i)}$ are straightforward. Specifically, $k_{\Delta\Theta_j}^{(i)}=\infty$ shall be set if no joint occurs at $x=x_j^{(i)}$ and, correspondingly, all terms in the 2nd row of matrices $\tilde{\mathbf{\Phi}}_{\mathbf{\Omega}_B}^{(i)}\left(x_j^{(i)}\right)$, $\tilde{\mathbf{\Phi}}_{\mathbf{J}_B}^{(i)}\left(x_j^{(i)},x_k^{(i)}\right)$ will vanish. In addition, terms in the 2nd column of matrix $\tilde{\mathbf{\Phi}}_{\mathbf{J}_B}^{(i)}\left(x_m^{(i)},x_j^{(i)}\right)$, shall be set equal to zero for all $x_m^{(i)}>x_j^{(i)}$. Likewise, if no mass-spring subsystem occurs at $x=x_j^{(i)}$, $\kappa_{B_j}^{(i)}(\omega)=0$ shall be set at $x=x_j^{(i)}$ and, in addition, terms in the 1st column of matrix $\tilde{\mathbf{\Phi}}_{\mathbf{J}_B}^{(i)}\left(x_m^{(i)},x_j^{(i)}\right)$ shall be set equal to zero for all $x_m^{(i)}>x_j^{(i)}$.

Finally, matrices $\tilde{\mathbf{\Gamma}}^{(i)}$ and $\mathbf{\Xi}^{(i)}$ are given as:

$$\tilde{\mathbf{\Gamma}}^{(i)} = \begin{bmatrix} \left(\tilde{\mathbf{W}}_A^{(i)}(0)\right)_1 & \mathbf{0}_{1\times4} \\ \mathbf{0}_{1\times2} & \left(\tilde{\mathbf{W}}_B^{(i)}(0)\right)_1 \\ \mathbf{0}_{1\times2} & \left(\tilde{\mathbf{W}}_B^{(i)}(0)\right)_2 \\ \left(\tilde{\mathbf{W}}_A^{(i)}\left(L^{(i)}\right)\right)_1 & \mathbf{0}_{1\times4} \\ \mathbf{0}_{1\times2} & \left(\tilde{\mathbf{W}}_B^{(i)}\left(L^{(i)}\right)\right)_1 \\ \mathbf{0}_{1\times2} & \left(\tilde{\mathbf{W}}_B^{(i)}\left(L^{(i)}\right)\right)_2 \end{bmatrix} \qquad \mathbf{\Xi}^{(i)} = \begin{bmatrix} -\left(\tilde{\mathbf{W}}_A^{(i)}(0)\right)_2 & \mathbf{0}_{1\times4} \\ \mathbf{0}_{1\times2} & -\left(\tilde{\mathbf{W}}_B^{(i)}(0)\right)_4 \\ \mathbf{0}_{1\times2} & \left(\tilde{\mathbf{W}}_B^{(i)}(0)\right)_3 \\ \left(\tilde{\mathbf{W}}_A^{(i)}\left(L^{(i)}\right)\right)_2 & \mathbf{0}_{1\times4} \\ \mathbf{0}_{1\times2} & \left(\tilde{\mathbf{W}}_B^{(i)}\left(L^{(i)}\right)\right)_4 \\ \mathbf{0}_{1\times2} & -\left(\tilde{\mathbf{W}}_B^{(i)}\left(L^{(i)}\right)\right)_3 \end{bmatrix} \tag{A.14a,b}$$

More details on the derivation of Eq.(A.1) through Eqs.(A.14) of this Appendix may be found in ref. [45] of the author.

9. REFERENCES

[1] J.R. Banerjee, Free vibration of beams carrying spring-mass systems. A dynamic stiffness approach, Comput. Struct. 104-105 (2012) 21-26.

[2] Y. Xiao, J. Wen, D. Yu, X. Wen, Flexural wave propagation in beams with periodically attached vibration absorbers: Band-gap behavior and band formation mechanisms, J. Sound Vib. 332 (2013) 867-893.

[3] Y. Liu, D. Yu, L. Li, H. Zhao, J. Wen, X. Wen, Design guidelines for flexural wave attenuation of slender beams with local resonators, Phys. Lett. A 362 (2007) 344-347.

[4] N. Nematipoor, M.R. Ashory, E. Jamshidi, Imposing nodes for linear structures during harmonic excitations using SMURF method, Arch. Appl. Mech. 82 (2012) 631-642.

[5] P.D. Cha, Enforcing nodes at required locations in a harmonically excited structure using simple oscillators, J. Sound Vib. 279 (2005) 799-816.

[6] P.D. Cha, Specifying nodes at multiple locations for any normal mode of a linear elastic structure, J. Sound Vib. 250(5) (2002) 923-934.

[7] D. Zhou, T. Ji, Estimation of dynamic characteristics of a spring-mass-beam system, Shock Vib. 14 (2007) 271-282.

[8] D. Zhou, T. Ji, Dynamic characteristics of a beam and distributed spring-mass system, Int. J. Solids Struct. 43 (2006) 5555-5569.

[9] F.M. Hosseini, N. Baddour, Alternative admissible functions for natural frequencies and mode shapes of a beam with lumped attachments, Struct. 10 (2017) 59-75.

[10] P.D. Cha, Natural frequencies of a linear elastica carrying any number of sprung masses, J. Sound Vib. 247(1) (2001) 185-194.

[11] J.S. Wu, D.W. Chen, Free vibration analysis of a Timoshenko beam carrying multiple spring-mass systems by using the numerical assembly technique, Int. J. Numer. Methods Eng. 50(5) (2001) 1039-1058.

[12] C.A. Rossit, P.A.A. Laura, Free vibrations of a cantilever beam with a spring–mass system attached to the free end, Ocean Eng. 28(7) (2001) 933-939.

[13] M. Gurgoze, On the eigenfrequencies of a cantilever beam with attached tip mass and a spring-mass system, J. Sound Vib. 190 (1996) 149-162.

[14] S. Kukla, B. Posiadala, Free vibrations of beams with elastically mounted masses, J. Sound Vib. 175 (1994) 557-564.

[15] P.D. Cha, Alternative formulations to obtain the eigensolutions of a continuous structure to which spring-mass systems are attached, J. Sound Vib. 246(4) (2001) 741-750.

[16] J.W. Nicholson, L.A. Bergman, Free vibration of combined dynamical systems, J. Eng. Mech. 112(1) (1986) 20254.

[17] P.D. Cha, C. Pierre, Frequency analysis of a linear elastic structure carrying a chain of oscillators, J. Eng. Mech. 125(5) (1999) 587-591.

[18] S. Kukla, Application of Green functions in frequency analysis of Timoshenko beams with oscillators, J. Sound Vib. 205(3) (1997) 355-363.

[19] K. Alsaif, M.A. Foda, Vibration suppression of a beam structure by intermediate masses and springs, J. Sound Vib. 256(4) (2002) 629-645.

[20] K.H. Low, On the methods to derive frequency equations of beams carrying multiple masses, Int. J. Mech. Sci. 43 (2001) 871-881.

[21] K.H. Low, An equivalent-center method for quick frequency analysis of beams carrying a concentrated mass, Comput. Struct. 500(3) (1994) 409-419.

[22] J. Wang, P. Qiao, Vibration of beams with arbitrary discontinuities and boundary conditions, J. Sound Vib. 308 (2007) 12-27.

[23] H.Y. Lin, Y.C. Tsai, Free vibration analysis of a uniform multi-span beam carrying multiple spring–mass systems, J. Sound Vib. 302 (2007) 442-456.

[24] Z. Zhang, F. Chen, Z. Zhang, H. Hua, Vibration analysis of non-uniform Timoshenko beams coupled with flexible attachments and multiple discontinuities, Int. J. Mech. Sci. 80 (2014) 131-143.

[25] S.H. Farghaly, TA. El-Sayed, Exact free vibration of multi-step Timoshenko beam system with several attachments, Mech. Syst. Signal Process. 72-73 (2016) 525-546.

[26] J.S. Wu, B.H. Chang, Free vibration of axial-loaded multi-step Timoshenko beam carrying arbitrary concentrated elements using continuous-mass transfer matrix method, Eur. J. Mech. A/Solids 38 (2013) 20-37.

[27] M. Gürgöze, On the eigenfrequencies of longitudinally vibrating rods carrying a tip mass and spring-mass in-span, J. Sound Vib. 216(2) (1998) 295-308.

[28] S. Demirtaş, M. Gurgoze, Sensitivity analysis of an axially vibrating elastic rod with several lumped attachments, Int. J. Mech. Eng. Educ. 42(3) (2014) 209-232.

[29] Y.Q. Guo, W.Q. Chen, Dynamic analysis of space structures with multiple tuned mass dampers, Eng. Struct. 29 (2007) 3390-3403.

[30] Y.Q. Guo, W.Q. Chen, Y.H. Pao, Dynamic analysis of space frames: The method of reverberation-ray matrix and the orthogonality of normal modes, J. Sound Vib. 317 (2008) 716-738.

[31] J.R. Banerjee, Dynamic stiffness formulation for structural elements: A general approach, Comput. Struct. 63(1) (1997) 101-103.

[32] C.A.N. Dias, M. Alves, A contribution to the exact modal solution of in-plane beam structures, J. Sound Vib. 328 (2009) 586-606.

[33] C.A.N. Dias, M. Alves, A method to solve the nonlinear eigenvalue problem of Timoshenko plane frames with rigid offsets and end releases, J. Sound Vib. 332 (2013) 1372-1387.

[34] C.A.N. Dias, General exact harmonic analysis of in-plane Timoshenko beam structures, Lat. Am. J. Solids Struct. 11 (2014) 2171-2202.

[35] S. Caddemi, I. Caliò, The exact explicit dynamic stiffness matrix of multi-cracked Euler–Bernoulli beam and applications to damaged frame structures, J. Sound Vib. 332(12) (2013) 3049-3063.

[36] A. Greco, A. Pau, Damage identification in Euler frames, Comput. Struct. 92-93 (2012) 328-336.

[37] M. Donà, A. Palmeri, M. Lombardo, A. Cicirello, An efficient two-node finite element formulation of multi-damaged beams including shear deformation and rotatory inertia, Comput. Struct. 147 (2015) 96-106.

[38] S. Caddemi, I. Caliò, F. Cannizzaro, The dynamic stiffness matrix (DSM) of axially loaded multi-cracked frames, Mech. Res. Commun. 84 (2017) 90-97.

[39] I. Elishakoff, F. Hache, N. Challamel, Critical contrasting of three versions of vibrating Bresse–Timoshenko beam with a crack, Int. J. Solids Struct. 109 (2017) 143-151.

[40] A. Yavari, S. Sarkani, E.T. Moyer, On applications of generalized functions to beam bending problems, Int. J. Solids Struct. 37 (2000) 5675-5705.

[41] G. Falsone, The use of generalised functions in the discontinuous beam bending differential equation, Int. J. Eng. Educ. 18(3) (2002) 337-343.

[42] A. Burlon, G. Failla, F. Arena, Exact frequency response analysis of axially loaded beams with viscoelastic dampers, Int. J. Mech. Sci. 115-116 (2016) 370-384.

[43] S. Guo, J.R. Banerjee, On the dynamics of a cracked beam, in: Proceedings of the 50th AIAA/ASME/ASCE/AHS/ASC Struct., Struct. Dyn., Mater. Conf., 4-7 May 2009, Palm Springs, California (US).

[44] A. Labib, D. Kennedy, C. Featherston, Free vibration analysis of beams and frames with multiple cracks for damage detection, J. Sound Vib. 333 (2014) 4991-5003.

[45] G. Failla, An exact generalised function approach to frequency response analysis of beams and plane frames with the inclusion of viscoelastic damping, J. Sound Vib. 360 (2016) 171-202.

[46] F.W. Williams, W.H. Wittrick, An automatic computational procedure for calculating natural frequencies of skeletal structures, Int. J. Mech. Sci. 12 (1970) 781-791.

[47] S. Ilanko, F.W. Williams, Wittrick-Williams algorithm proof of bracketing and convergence theorems for eigenvalues of constrained structures with positive and negative penalty parameters, Int. J. Numer. Methods Eng. 75 (2008) 83-102.

[48] K.J. Bathe, Finite Element Procedures, 2nd ed., Prentice-Hall, Upper Saddle River, 2014.

[49] G. Oliveto, A. Santini, E. Tripodi, Complex modal analysis of a flexural vibrating beam with viscous end conditions, J. Sound Vib. 200(3) (1997) 327-345.

[50] A.S. Veletsos, C.E. Ventura, Modal analysis of non-classically damped linear systems. Earthq. Eng. Struct. Dyn. 14 (1986) 217-243.

[51] R.W. Clough, J. Penzien, Dynamics of Structures, 3rd ed., Computers & Structures, Berkeley, 2003.

[52] Mathematica, Version 7.0. Wolfram Research Inc., Champaign, 2008.

[53] ADINA, Version 9.3. ADINA R. & D. Inc., Watertown, 2017.

DECLARATIONS OF INTEREST: NONE.